JACS
JOURNAL OF THE AMERICAN CHEMICAL SOCIETY
Article
pubs.acs.org/JACS

Supramolecular Architectures with π-Acidic 3,6-Bis(2-pyridyl)-1,2,4,5-tetrazine Cavities: Role of Anion−π Interactions in the Remarkable Stability of Fe(II) Metallacycles in Solution

Helen T. Chifotides,* Ian D. Giles, and Kim R. Dunbar*

Department of Chemistry, Texas A&M University, College Station, Texas 77843, United States

Supporting Information

ABSTRACT: The comprehensive investigation reported herein provides compelling evidence that anion−π interactions are the main driving force in the formation of self-assembled Fe(II)-templated metallacycles with bptz [3,6-bis(2-pyridyl)-1,2,4,5-tetrazine] in high yields. It was demonstrated by X-ray crystallography, ^{1}H NMR, solution and solid-state MAS ^{19}F NMR spectroscopies, CV and MS studies that the anions $[X]^-$ = $[BF_4]^-$, $[ClO_4]^-$ and the anions $[Y]^-$ = $[SbF_6]^-$, $[AsF_6]^-$, $[PF_6]^-$ template molecular squares $[Fe_4(bptz)_4(CH_3CN)_8][X]_8$ and pentagons $[Fe_5(bptz)_5(CH_3CN)_{10}][Y]_{10}$, respectively. The X-ray structures of $[\{Fe_4(bptz)_4(CH_3CN)_8\}\subset BF_4][BF_4]_7$ and $[\{Fe_5(bptz)_5(CH_3CN)_{10}\}\subset 2SbF_6][SbF_6]_8$ revealed that the $[BF_4]^-$ and $[SbF_6]^-$ anions occupy the π-acidic cavities, establishing close directional F···$C_{tetrazine}$ contacts with the tetrazine rings that are by ∼0.4 Å shorter than the sum of the F···C van der Waals radii ($\sum R_{vdW}$ F···C = 3.17 Å). The number and strength of F···$C_{tetrazine}$ contacts are maximized; the F···$C_{tetrazine}$ distances and anion positioning versus the polygon opposing tetrazine rings are in agreement with DFT calculations for $C_2N_4R_2$···$[X]^-$···$C_2N_4R_2$ (R = F, CN; $[X]^-$ = $[BF_4]^-$, $[PF_6]^-$). In unprecedented solid-state ^{19}F MAS NMR studies, the templating anions, engaged in anion−π interactions in the solid state, exhibit downfield chemical shifts $\Delta\delta(^{19}F) \approx 3.5-4.0$ ppm versus peripheral anions. NMR, CV, and MS studies also establish that the Fe(II) metallacycles remain intact in solution. Additionally, interconversion studies between the Fe(II) metallacycles in solution, monitored by ^{1}H NMR spectroscopy, underscore the remarkable stability of the metallapentacycles $[Fe_5(bptz)_5(CH_3CN)_{10}][PF_6]_{10} \ll [Fe_5(bptz)_5(CH_3CN)_{10}][SbF_6]_{10} < [Fe_5(bptz)_5(CH_3CN)_{10}][AsF_6]_{10}$ versus $[Fe_4(bptz)_4(CH_3CN)_8][BF_4]_8$, given the inherent angle strain in five-membered rings. Finally, the low anion activation energies of encapsulation ($\Delta G^{\ddagger} \approx 50$ kJ/mol), determined from variable-temperature ^{19}F NMR studies for $[Fe_5(bptz)_5(CH_3CN)_{10}][PF_6]_{10}$ and $[Zn_4(bptz)_4(CH_3CN)_8][BF_4]_8$, confirm anion encapsulation in the π-acidic cavities by anion−π contacts (∼20−70 kJ/mol).

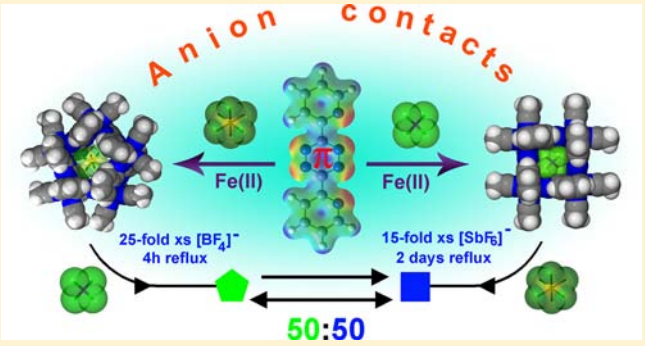

INTRODUCTION

Coordination-driven self-assembly,[1−4] a topic at the frontier of supramolecular chemistry,[5,6] harnesses the structural versatility of metal ions and the directionality of metal−ligand interactions to promote the spontaneous assembly of elegant supramolecular achitectures,[1,3,7−9] endowed in some instances with unusual properties and ingenious applications[10−14] or intriguing host−guest behavior.[15−17] This fascinating synthetic strategy has led to a myriad of metallacyclic architectures, ranging from molecular triangles to cages, capsules, and various polyhedra[7] and to many examples of the most common nuclearity structures, namely, molecular squares.[1,3,4] In pioneering studies by Stang et al.[1] and Fujita et al.[3a] transition metals with 90° L−M−L bonds (where L is a ligand), which are compatible with square angles, were incorporated as building blocks into the first square frameworks and, when combined with the appropriate organic linkers, led to an abundance of conformationally stable molecular squares and rectangles.[1] In contrast to this situation is the challenge of constructing pentagons, due to the scarcity of 108° subunits and the incongruity between octahedral L−M−L and internal pentagon angles (108°), both of which contribute to their inherent lower stability as compared to squares.[18] These factors have contributed to a dearth of reported pentagonal architectures, with the exceptions of a handful of self-assembled pentameric metallacycles detected by mass spectrometry,[18,19] an anion-templated pentanuclear circular helicate,[20] a molecular pentafoil knot,[21] and very recently a remarkable unprecedented self-assembled pentagonal prism.[22]

Apart from the directing elements imposed by the building blocks, the outcome of the self-assembly reactions can be controlled by external factors such as synthon concentration, solvent, counterions, or the presence of a template. A template is a directing element that induces or selectively stabilizes a desired assembly through noncovalent interactions, during a

Received: August 24, 2012
Published: February 18, 2013

   dx.doi.org/10.1021/ja3082473 | J. Am. Chem. Soc. 2013, 135, 3039−3055

delicately balanced thermodynamically controlled self-assembly process;[23] in essence, this means that the template tips the scales in favor of the emergence of a single preferred product, at the expense of other potential products that can form from the reactants.[24] The strategy of exposing the system to a template to favor a desired supramolecular entity is an extremely important tool in supramolecular chemistry, with the impact on the self-assembly reaction outcome underscored in several notable paradigms.[20,25−28] The template can be a temporary or permanent helper, but its presence, however fleeting, is always necessary for the formation of the final product and essential for its integrity in some cases.[23,24] From a structural point of view, the size and geometry of the template are important in targeting the desired templated product, whereas in terms of electrostatics, the template can be cationic, neutral, or anionic. Despite the extensive use of cationic templates, the ability of anions to operate as templates (or guests) and direct the course of an assembly process through noncovalent interactions was not fully appreciated until recently.[24,29a,30a,31] Anion binding typically involves noncovalent interactions, such as hydrogen-bonding, electrostatic, $\pi-\pi$ stacking, and other van der Waals forces,[29b] but recently, another novel noncovalent attractive force involving anions and π-acidic (or electron-deficient) charge-neutral aromatic rings, namely, the anion$-\pi$ interaction,[32−36] has become a topic of great interest. The pioneering theoretical studies[37−39] that established the favorable nature of anion$-\pi$ interactions (~20−70 kJ/mol), albeit at first glance counterintuitive, were complemented by an ever-increasing arsenal of experimental evidence for their presence in the solid state[40−53] and in solution,[30b,54−58] as well as additional theoretical studies[59−62] that lend further insight into aspects of the interaction. Currently, the area of anion$-\pi$ research is highly topical in the scientific community,[32−36] from both the fundamental point of view and the promise that anion$-\pi$ interactions hold for the design of novel colorimetric sensors,[63,64] highly selective anion receptors,[29a,54,65,66] selective hosts[67] for anion recognition[29a,35,57,68] and anion transport,[69] as well as their likely involvement in biological functions.[69,70]

Armed with the aforementioned information and our early findings involving anion encapsulation in Ni(II) metallacycles,[71−73] gleaned from X-ray crystallography and mass spectrometry experiments, we launched a comprehensive investigation of anion-templated self-assembly reactions between solvated Fe(II) metal ions and the divergent π-acidic bis-bipyridine ligand 3,6-bis(2-pyridyl)-1,2,4,5-tetrazine (bptz; Chart 1). Herein, we report the preparation and characterization of the anion-templated molecular squares $[Fe_4(bptz)_4(CH_3CN)_8][X]_8$ ($[X]^-$ = $[BF_4]^-$, $[ClO_4]^-$) and pentagons $[Fe_5(bptz)_5(CH_3CN)_{10}][Y]_{10}$ ($[Y]^-$ = $[SbF_6]^-$, $[AsF_6]^-$, $[PF_6]^-$), featuring π-acidic cavities, in high yields. In the molecular metallapentacycle $[\{Fe_5(bptz)_5(CH_3CN)_{10}\}\subset 2SbF_6][SbF_6]_8$,[74] which was reported in preliminary communication form, the anion$-\pi$ contacts are evidenced by X-ray crystallography. In the current work, we report, for the first time, studies involving anion$-\pi$ interactions by ^{19}F magic-angle-spinning (MAS) nuclear magnetic resonance (NMR) spectrometry as well as density functional theory (DFT) calculations, results that support the strategic nature of the anion positioning and the additive anion$-\pi$ contacts in the aforementioned π-acidic metallacycle cavities. The notable stability of the polygons in solution was probed by ^1H NMR spectroscopy and cyclic voltammetry, as well as by mass spectrometry. Finally, unprecedented NMR studies on the metallacycles in solution clearly support the contention that the anions play a decisive role in their formation and stability and provide unequivocal evidence for templation *only* in the presence of specific anions.

Chart 1

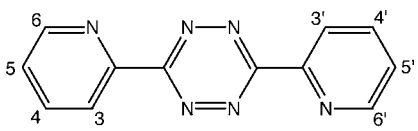

bptz

EXPERIMENTAL DETAILS

Materials. The ligand 3,6-bis(2-pyridyl)-1,2,4,5-tetrazine (bptz) was prepared by a literature procedure[75] and recrystallized from benzene. The fully solvated white metal salts $[Fe(CH_3CN)_6][X]_2$ (X = $[BF_4]^-$, $[SbF_6]^-$) were prepared from literature procedures by reacting Fe(s) with the nitrosonium salts of the corresponding anions and stored in the drybox.[76] The salt $Fe(ClO_4)_2{\cdot}2H_2O$ was purchased from Aldrich and used without further purification. (***Caution!*** *Perchlorate salts of metal complexes with organic ligands are potential explosives. Although we have encountered no incidents in the preparation and studies of the salts, it is advisible to use only small amounts and to handle the compounds with caution in the presence of wet solvents.*) The salts $[n\text{-}Bu_4N][BF_4]$, $[n\text{-}Bu_4N][PF_6]$, and $KAsF_6$ were purchased from Alfa-Aesar or Aldrich and used without further purification under dry conditions. The salt $[n\text{-}Bu_4N][SbF_6]$ was prepared by metathesis of $NaSbF_6$ and $[n\text{-}Bu_4N][Cl]$ in H_2O, recrystallized from ethyl acetate, and precipitated with pentane. All reactions were performed in the drybox or under an atmosphere of dry N_2 with the use of Schlenk-line procedures. All of the samples for the NMR measurements in solution and the solid state were prepared in the drybox. Airtight NMR tubes equipped with a J. Young valve were used for the acquisition of all NMR data for the Fe(II) compounds in solution to prevent oxidation. All solvents were dried by standard methods, distilled under nitrogen, and deoxygenated prior to use. Anhydrous acetonitrile was purchased from Aldrich and used for the electrochemistry studies. Anhydrous deuterated CD_3CN-d_3 was purchased from CIL.

Physical Measurements. Please see the Supporting Information.

Syntheses. *$[\{Fe_4(bptz)_4(CH_3CN)_8\}\subset BF_4][BF_4]_7$ (**1**).* A magenta solution of bptz (283 mg, 1.20 mmol) in CH_3CN (30 mL) was slowly added with stirring to a colorless solution of $[Fe(CH_3CN)_6][BF_4]_2$ (576 mg, 1.21 mmol) in CH_3CN (40 mL); an immediate color change of the reaction solution to dark blue ensued. After overnight stirring, a small quantity of $[n\text{-}Bu_4N][BF_4]$ (20 mg) was added to the solution, which was subsequently separated into two portions and layered over either toluene or dichloromethane. After several days, analytically pure solid was removed by filtration and dried under anaerobic conditions. Yield: 233 mg (81%). Anal. Calcd for $Fe_4C_{64}N_{32}H_{56}B_8F_{32}{\cdot}4CH_2Cl_2{\cdot}CH_3CN$: C, 32.65; N, 17.96; H, 2.60%. Found: C, 32.69; N, 18.14; H, 2.63%. ^1H NMR in CD_3CN (δ, ppm): 7.61 (d, 8H, 3,3′-H), 8.05 (td, 8H, 5,5′-H), 8.27 (td, 8H, 4,4′-H), 8.89 (d, 8H, 6,6′-H), 1.95 (24H, s, CH_3CN). UV−vis (CH_3CN) λ/nm (ε/$[M^{-1}\ cm^{-1}]$): 797 (19000). Cyclic voltammetry (CV; CH_3CN, versus Ag/AgCl): $E_{1/2}$(ox): −0.094, +0.047, +0.32, +0.52 V (reversible). Electrospray ionization Fourier transform ion cyclotron resonance mass spectrometry (ESI-FT-ICR-MS; m/z): 2155.01 for $[Fe_4(bptz)_4(CH_3CN)_6(CD_3CN)(BF_4)_8 + H^+]^+$ (NMR sample dissolved in CD_3CN; Figure S1).

*$[\{Fe_5(bptz)_5(CH_3CN)_{10}\}\subset 2SbF_6][SbF_6]_8$ (**2**).* A magenta solution of bptz (169 mg, 0.716 mmol) in CH_3CN was slowly added to a colorless solution of $[Fe(CH_3CN)_6][SbF_6]_2$ (554 mg, 0.716 mmol) in CH_3CN, resulting in an immediate color change of the solution to dark blue. The reaction solution was layered with toluene after stirring overnight to yield a dark blue analytically pure solid, which was filtered and dried

dx.doi.org/10.1021/ja3082473 | J. Am. Chem. Soc. 2013, 135, 3039−3055

under anaerobic conditions. Yield: 555 mg (90%). Anal. Calcd for $Fe_5C_{80}N_{40}H_{70}Sb_{10}F_{60}\cdot C_7H_8$: C, 24.18; N, 12.96; H, 1.84%. Found: C, 24.40; N, 13.28; H, 1.96%. ^{1}H NMR in CD_3CN (δ, ppm): 7.52 (d, 10H, 3,3′-H), 8.07 (td, 10H, 5,5′-H), 8.31 (td, 10H, 4,4′-H), 8.82 (d, 10H, 6,6′-H), 1.95 (30H, s, CH_3CN). UV−vis (CH_3CN) λ/nm (ε/[M^{-1} cm^{-1}]): 802 (30000). CV (CH_3CN, versus Ag/AgCl): $E_{1/2}$(ox): −0.027, +0.034, +0.37, +0.56 V (reversible). ESI-FT-ICR-MS (m/z): 1774.83 for $[Fe_5(bptz)_5(CH_3CN)_5(SbF_6)_8-2H]^{2+}$ (Figure S2).[74]

$[Fe(CH_3CN)_6][PF_6]_2$. A white suspension of $TlPF_6$ (100 mg, 0.286 mmol) in CH_3CN (10 mL) was added to a purple/brown solution of FeI_2 (44.3 mg, 0.143 mmol) in CH_3CN (10 mL). Precipitation of yellow TlI ensued immediately. The reaction mixture was stirred overnight in a drybox, the resulting yellow precipitate was removed by filtration, and the solution was filtered again several times through dry Celite to remove fine particles. The almost-colorless solution was reduced in volume to ∼6 mL on a vacuum line, and diethyl ether was slowly added to produce a cloudy solution from which colorless needle-like crystals formed. The flask was placed in the refrigerator for three days in a drybox, and the white solid that formed was removed by filtration, washed with diethyl ether (3 × 3 mL), and dried under a vacuum. Yield: 57 mg (67%). ^{19}F NMR in CD_3CN (δ, ppm): −71.6 ppm (free $[PF_6]^-$ ions). IR (Nujol mull, CsI, cm^{-1}): (CH_3CN) $\nu_{C\equiv N}$ 2325 (s), 2293 (s); ($[PF_6]^-$) ν_{PF6} 875 (vs), 558(s).

*$[Fe_5(bptz)_5(CH_3CN)_{10}][PF_6]_{10}$ (**3**).* A magenta solution of bptz (76.4 mg, 0.323 mmol) in CH_3CN (15 mL) was slowly added to a colorless solution of $[Fe(CH_3CN)_6][PF_6]_2$ (191.5 mg, 0.323 mmol) in CH_3CN (15 mL), resulting in an immediate color change of the solution to dark blue. Layering the reaction solution with either toluene or dichloromethane, after it had been stirred overnight and separated into two portions, afforded a dark blue solid, which was filtered and dried under anaerobic conditions. Yield: 134 mg (64%). Anal. Calcd for $Fe_5C_{80}N_{40}H_{70}P_{10}F_{60}\cdot 4CH_2Cl_2$: C, 27.56; N, 15.31; H, 2.15%. Found: C, 27.56; N, 15.40; H, 2.31%. ^{1}H NMR in CD_3CN (δ, ppm): 7.52 (d, 10H, 3,3′-H), 8.06 (td, 10H, 5,5′-H), 8.33 (td, 10H, 4,4′-H), 8.84 (d, 10H, 6,6′-H), 1.95 (30H, s, CH_3CN). UV−vis (CH_3CN) λ/nm (ε/[M^{-1} cm^{-1}]): 828 (19040), 607 (15670). CV (CH_3CN, versus Ag/AgCl): $E_{1/2}$(ox): −0.085, +0.039, +0.32, +0.55 V. ESI-FT-ICR-MS (m/z): 1046.17 for $[Fe_5(bptz)_5(CH_3CN)_9(PF_6)_9 + 2H^+]^{3+}$ (Figure S3).

*$[Fe_5(bptz)_5(CH_3CN)_{10}][AsF_6]_{10}$ (**4**).* A magenta solution of bptz (49 mg, 0.207 mmol) in CH_3CN (15 mL) was added to an off-white/light tan suspension of $Fe(CF_3SO_3)_2$ (70 mg, 0.198 mmol) in CH_3CN (15 mL) under a N_2 atmosphere, resulting in an immediate color change of the solution to dark blue. The reaction solution was stirred for 15 min, and a 3-fold excess of $KAsF_6$ (144 mg, 0.633 mmol) was subsequently added. The reaction mixture was stirred overnight, and the solution was layered over toluene, which produced a dark blue solid at the bottom of the flask after two days. Yield: 122 mg (82%). Anal. Calcd for $Fe_5C_{80}N_{40}H_{70}As_{10}F_{60}\cdot 4CH_3CN\cdot 2C_7H_8$: C, 29.81; N, 15.00; H, 2.40%. Found: C, 29.55; N, 15.19; H, 2.31%. ^{1}H NMR in CD_3CN (δ, ppm): 7.48 (d, 10H, 3,3′-H), 8.04 (td, 10H, 5,5′-H), 8.30 (td, 10H, 4,4′-H), 8.85 (d, 10H, 6,6′-H), 1.95 (30H, s, CH_3CN). UV−vis (CH_3CN) λ/nm (ε/[M^{-1} cm^{-1}]): 768 (29240), 711 (20290), 517 (7246). CV (CH_3CN, versus Ag/AgCl): $E_{1/2}$(ox): − 0.090, +0.040, +0.34, + 0.58 V (reversible). ESI-FT-ICR-MS (m/z): 1507.3 for $[Fe_5(bptz)_5(CH_3CN)(AsF_6)_8]^{2+}$ (Figure S4).

*$[Fe_4(bptz)_4(CH_3CN)_8][ClO_4]_8$ (**5**): Small Scale Synthesis for NMR Studies.* A magenta solution of bptz (13 mg, 0.055 mmol) in CD_3CN (0.75 mL) was added to a solution of $Fe(ClO_4)_2\cdot 2H_2O$ (16 mg, 0.055 mmol) in CD_3CN (0.75 mL), resulting in an immediate color change of the solution to dark blue. The reaction solution was stirred for a short time, and the spectra were recorded. ^{1}H NMR in CD_3CN (δ, ppm): 7.66 (d, 8H, 3,3′-H), 8.02 (td, 8H, 5,5′-H), 8.27 (td, 8H, 4,4′-H), 8.88 (d, 8H, 6,6′-H), 1.95 (24H, s, CH_3CN). ESI-FT-ICR-MS (m/z): 882.87 for $[Fe_4(bptz)_4(ClO_4)_7 + 2H^+]^{3+}$ (Figure S5).

X-ray Crystallography. Single-crystal X-ray data for **1** and **2** were collected on a Bruker APEX II CCD X-ray diffractometer equipped with a graphite-monochromated Mo Kα radiation source (λ = 0.71073 Å). Dark blue crystals of **1** and **2** were affixed as quickly as possible to a nylon loop with Paratone oil and placed in a N_2(g) cryostream at 163(2) K to minimize exposure to air. The crystal parameters and information pertaining to the data collection, solution, and refinement of the crystals for **1**·9CH_3CN and **2**·8.5CH_3CN are detailed in the Supporting Information and summarized in Table S1. Selected bond distances and angles are provided in the figure captions and Tables S2 and S3. Numerous efforts to crystallize $[Fe_5(bptz)_5(CH_3CN)_{10}][PF_6]_{10}$ invariably led to poorly diffracting crystals even when the data were acquired with synchrotron radiation.

*$[\{Fe_4(bptz)_4(CH_3CN)_8\}\subset BF_4][BF_4]_7\cdot 9CH_3CN$, **1**·9$CH_3CN$.* Dark blue plate-like crystals were grown by layering an acetonitrile solution of **1** over toluene. Compound **1** crystallizes in the triclinic system, space group $P\bar{1}$. The $[BF_4]^-$ anion residing in the cavity of the square is equally disordered over two positions. The electron density corresponding to nine highly disordered solvent molecules observed during the data refinement was removed using the SQUEEZE[77] routine implemented in PLATON.[78]

*$[\{Fe_5(bptz)_5(CH_3CN)_{10}\}\subset 2SbF_6][SbF_6]_8\cdot 8.5CH_3CN$, **2**·8.5$CH_3CN$.* Dark blue plate-like crystals were grown by layering an acetonitrile solution of compound **2** over toluene. Compound **2** crystallizes in the orthorhombic system, space group *Pbcn*. There are two symmetry-related $[SbF_6]^-$ anions in close proximity in the cavity of **2**. The electron density corresponding to 8.5 disordered solvent molecules observed during the data refinement was removed using the SQUEEZE[77] routine implemented in PLATON.[78]

Theoretical Calculations. Density functional theory (DFT) computations were undertaken for 3,6-difluoro- and dicyanotetrazine with the $[BF_4]^-$ and $[PF_6]^-$ anions, as well as for the corresponding double-ring/single-anion systems. The calculations were performed in Gaussian 09, revision B.01,[79] with the B3LYP hybrid functional incorporating the Becke three-parameter (B3) exchange functional[80] and the correlation functional of Lee, Yang, and Parr (LYP)[81] with the Pople-type basis set 6-31+G(d),[82] incorporating diffuse orbital and polarization functions on non-hydrogen atoms [B3LYP/6-31+G(d)]. For the single-ring/anion calculations, the basis set superposition errors (BSSEs)[83] were calculated and were negligible.[84] Unrestricted geometry optimizations of one arene with one anion as well as the individual anions and arenes were performed on a 128-processor Altix 3700 with Itanium^2 Madison processors. Unrestricted geometry optimizations of two arenes with one anion were performed on an IBM iDataplex Cluster comprising 372 nodes based on Intel's 64-bit Nehalem and Westmere processor architecture. Frequency computations were performed on the final geometry-optimized structures to ensure that a minimum had been reached, as determined by the absence of imaginary frequencies. Results were analyzed and images were generated using the Agui graphical user interface.[85]

RESULTS

X-ray Crystallography. *$[\{Fe_4(bptz)_4(CH_3CN)_8\}\subset BF_4][BF_4]_7\cdot 9CH_3CN$.* The thermal ellipsoid and the space-filling plots for **1** are provided in Figures 1 and 2, respectively. The four Fe(II) ions and bptz ligands form a molecular square in which each metal ion occupies a vertex and each ligand spans one edge as a bridge between the metal centers. The coordination geometry of the Fe(II) ions is octahedral with four sites being occupied by two chelating bptz N-donor ligands, in an *anti* orientation, with the remaining positions being filled by two CH_3CN molecules. The Fe−N distances are in the range of 1.86−1.97 Å (Table S2), which indicates low-spin (LS) Fe(II) centers (the Fe−N bond lengths can be used as an indicator of the spin state, because the population of the antibonding e_g in the high spin (HS) center causes elongation of the bond length by about 0.2 Å),[10c,86] whereas the N−Fe−N angles are in the range 80.9−97.0°. The Fe···Fe cross-ligand distances are ∼6.45 Å, and the Fe···Fe cross-cavity distances are 9.23 and 9.02 Å. The Fe···Fe···Fe angles are 88.6° and 91.3°, which are close to the ideal 90° angles required for a square. The cavity of **1** contains a tightly encapsulated $[BF_4]^-$ anion

dx.doi.org/10.1021/ja3082473 | J. Am. Chem. Soc. 2013, 135, 3039−3055

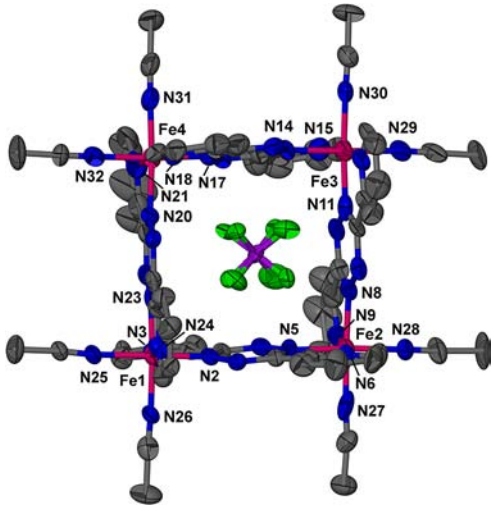

Figure 1. Thermal ellipsoid plot of the cationic unit $[Fe_4(bptz)_4(CH_3CN)_8 \subset BF_4]^{7+}$ in **1** at the 50% probability level. Selected bond distances (Å) and angles (deg): Fe1–N2 1.893(5), Fe1–N23 1.901(6), Fe2–N5 1.900(6), Fe2–N9 1.963(7), Fe3–N15 1.960(8), Fe3–N11 1.860(7), Fe4–N18 1.950(7), Fe4–N21 1.922(7), N2–Fe1–N23 92.7(2), N5–Fe2–N9 91.6(3), N30–Fe3–N15 90.8, N21–Fe4–N32 92.0(3), Fe···Fe···Fe 88.6 and 91.3. Atom colors: Fe, fuschia; C, dark gray; N, blue; B, purple; F, green.

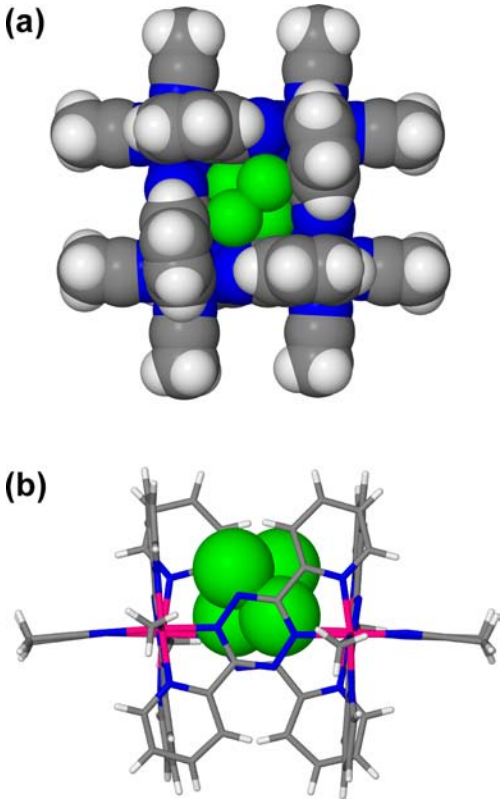

Figure 2. (a) Space-filling front-view representation of the cavity of $[Fe_4(bptz)_4(CH_3CN)_8 \subset BF_4]^{7+}$ depicting the tight packing of the encapsulated $[BF_4]^-$ anion. (b) Side view of the cavity with the anion depicted with space-filling spheres. Atom colors: Fe, fuschia; C, dark gray; N, blue; B, purple; F, green; H, white.

(Figure 2), which is disordered equally over two positions and is poised to establish close F···C contacts with the C atoms of two opposing bptz tetrazine rings (for every position) at the following distances: F1A···C6 2.923(9), F2A···C7 2.861(9), F3A···C30 2.883(9), F4A···C31 2.835(9), F1B···C43 2.742(2), F2B···C18 2.951(16), F3B···C19 2.780(2), and F4B···C42 2.798(2) (Figure 3). The aforementioned F···$C_{tetrazine}$ distances

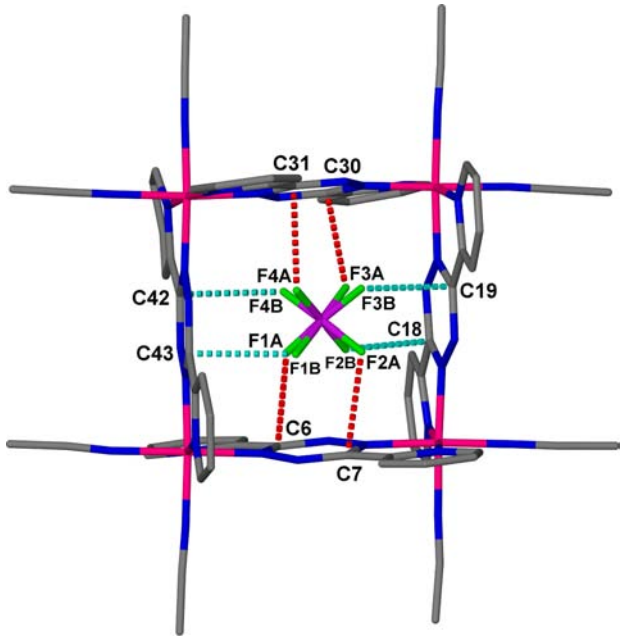

Figure 3. Stick representation of the cationic unit $[Fe_4(bptz)_4(CH_3CN)_8 \subset BF_4]^{7+}$ in **1**. Anion–π contacts are depicted with red and teal dashed lines; the two colors correspond to the two positions of disorder for the anion.

are up to 0.43 Å shorter than the sum of the van der Waals radii, $\sum R_{vdW}$ F···C = 3.17 Å. Regarding the outer-sphere $[BF_4]^-$ anions, four are located around the periphery of the square metallacycle, close to the tetrazine and pyridyl rings of the cationic unit, and establish several short anion–π contacts with the C atoms (e.g., for $[BF_4]_{ext}^-$···$C_{tetrazine}$: F13···C30 2.845(10), F17···C42 2.892(8), F5···C6 2.937(8) Å; for $[BF_4]_{ext}^-$···$C_{pyridyl}$: F20···C41 2.942(11) Å; Figure S6). The remaining three anions are located between the cationic units along with solvent molecules (Figure S7).

$[\{Fe_5(bptz)_5(CH_3CN)_{10}\} \subset 2SbF_6][SbF_6]_8 \cdot 8.5CH_3CN$. The essential features of the molecular structure of **2** were reported in a previous communication.[74] A thermal ellipsoid plot and a packing diagram of **2** are provided in Figures 4 and S8, respectively. The molecular cation consists of a pentagon in which the metal ions occupy the apices and the five bptz ligands span the edges of the polygon. Two different cis chelating bptz N-donor moieties, in an anti orientation, and two CH_3CN molecules compose the octahedral environment of each Fe(II) ion. The interatomic Fe–N distances are in the range of 1.87–2.00 Å (Table S3), which indicate LS Fe(II) centers as in the case of **1**.[86] The Fe···Fe···Fe vertex angles correspond to an ideal pentagon (108°) despite the fact that the N–Fe–N coordination angles at the vertices are close to 90°. These two essential geometrical requirements are met owing to the flexibility of the bptz bridging ligands; the tetrazine rings bow inward and do not lie in the same plane as the two outer pyridyl rings (average dihedral angles ~8°) to alleviate angle strain and allow for the formation of the closed pentagonal structure.[74]

There are two symmetry-related $[SbF_6]^-$ anions in close proximity in the cavity of **2** (Figures 4 and S9A), which is

dx.doi.org/10.1021/ja3082473 | J. Am. Chem. Soc. 2013, 135, 3039–3055

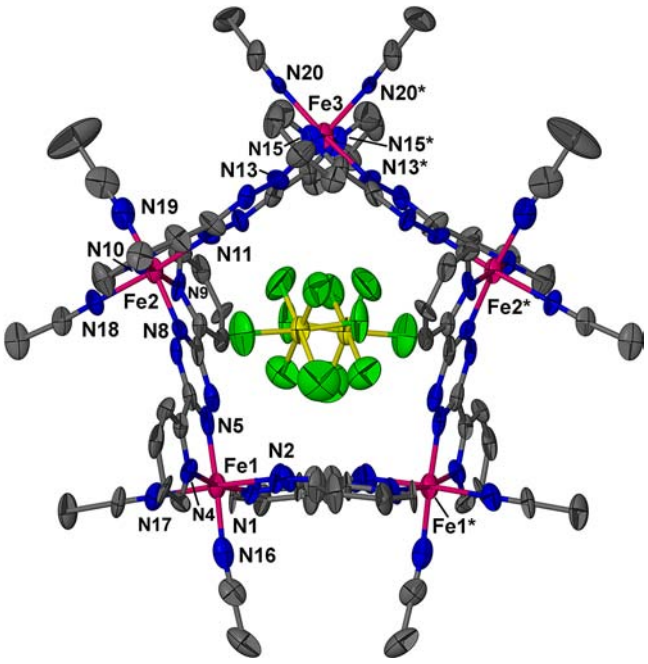

Figure 4. Thermal ellipsoid of the cationic unit $[\{Fe_5(bptz)_5(CH_3CN)_{10}\}\subset 2SbF_6]^{8+}$ in **2**, at the 50% probability level, depicted with the two encapsulated $[SbF_6]^-$ anions. Selected bond distances (Å) and angles (deg): Fe1−N1 1.96(1), Fe1−N2 1.90(1), Fe1−N4 1.963(12), Fe2−N8 1.872(12), Fe2−N9 2.007(13), Fe2−N10 1.959(11), Fe2−N11 1.884(11), Fe3−N13 1.868(11), Fe3−N15 1.972(11); N1−Fe1−N5 92.9(5), N2−Fe1−N5 93.9(5), N11−Fe2−N8 95.4(5), N11−Fe2−N9 92.5(5), Fe1···Fe2···Fe3 109.2, Fe1···Fe1*···Fe2* 107.5, Fe2···Fe3···Fe2* 106.5. Atom colors: Fe, fuschia; C, dark gray; N, blue; Sb, yellow; F, green.

unusual but not unprecedented for metallacyclic cages.[87−90] The two encapsulated $[SbF_6]^-$ anions fit tightly within the cavity of **2**, and each anion engages in three short F···$C_{tetrazine}$ contacts with the tetrazine rings of the bptz entities (each anion is disordered between two positions: $[SbF_6]^-$···$C_{tetrazine}$, F10···C13 2.81(2), F12A···C12 2.83(3), F14A···C25 2.89(3), F14···C24 2.93(2), F10A···C13 2.96(3), F12···C12 3.03(2) Å), as well as in longer F···C contacts F10A···C6 3.35(3), F12···C6 3.37(2) Å (Figure S9A).[74] The aforementioned F···$C_{tetrazine}$ distances are up to 0.36 Å shorter than $\sum R_{vdW}$ F···C (3.17 Å). The remaining eight $[SbF_6]^-$ anions are located around the external periphery of the cationic unit. In **2**, close contacts, up to 0.32 Å shorter than $\sum R_{vdW}$ C···F, are also observed between the peripheral $[SbF_6]^-$ anion F atoms and the tetrazine or pyridyl rings of the bptz entities (Figure S9B). For example, for $[SbF_6]_{ext}^-$···$C_{tetrazine}$, the distances are F18···C24 2.848, F6···C12 2.943, F2···C13 3.105 Å (colored dotted lines), and for $[SbF_6]_{ext}^-$···$C_{pyridyl}$, they are F3···C15 2.855, F5···C10 2.942, F17···C22 = 2.936 Å (black dotted lines). Compound **2** exhibits a corrugated packing of the pentagon units along the *b* and *c* axes with interstitial anions and solvent molecules occupying the intermolecular voids; the pentagonal metallacycles are aligned along the *a* axis (Figure S8).

NMR Spectroscopic Studies in Solution. ^{1}H NMR Spectroscopy of the Fe(II) Metallacycles. The aromatic region of the ^{1}H NMR spectrum of free bptz in CD_3CN exhibits resonances at δ 8.93 (6,6′), 8.64 (3,3′), 8.10 (4,4′), and 7.65 (5,5′) ppm for the protons of the pyridyl rings (Figure 5a).[73] The ^{1}H NMR spectra of the Fe(II) metallacycles exhibit the expected number of resonances for symmetrically

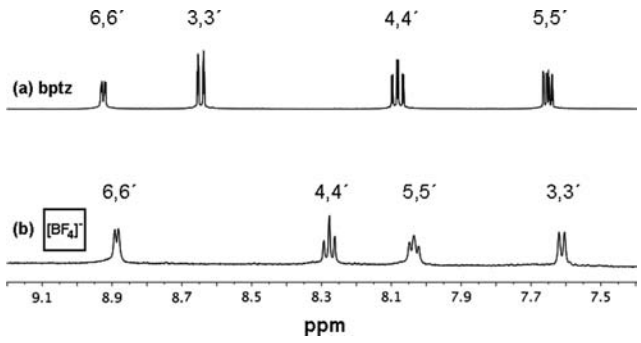

Figure 5. ^{1}H NMR spectra in CD_3CN of (a) free bptz and (b) $[Fe_4(bptz)_4(CH_3CN)_8][BF_4]_8$.

coordinated bptz ligands. The aromatic region of the ^{1}H NMR spectrum for the square $[Fe_4(bptz)_4(CH_3CN)_8][BF_4]_8$ (Figure 5b) in CD_3CN exhibits four sets of resonances, indicating that each bptz ligand is bridging two metal centers and that the two bptz pyridyl groups are equivalent. The resonances at δ 7.61, 8.05, 8.27, and 8.89 ppm are ascribed to the 3,3′-, 5,5′-, 4,4′-, and 6,6′-H of the pyridyl rings, respectively (Figure 5b, Table 1). The resonances for protons

Table 1. ^{1}H NMR Resonances for Free bptz and the Fe(II) Metallacycles in CD_3CN

compound	δ (ppm)			
	3,3′-H	5,5′-H	4,4′-H	6,6′-H
bptz	8.64	7.65	8.10	8.93
$[Fe_4(bptz)_4(CH_3CN)_8][BF_4]_8$	7.61	8.05	8.27	8.89
$[Fe_4(bptz)_4(CH_3CN)_8][ClO_4]_8$	7.66	8.02	8.27	8.88
$[Fe_5(bptz)_5(CH_3CN)_{10}][SbF_6]_{10}$	7.52	8.07	8.31	8.82
$[Fe_5(bptz)_5(CH_3CN)_{10}][PF_6]_{10}$	7.52	8.06	8.33	8.84
$[Fe_5(bptz)_5(CH_3CN)_{10}][AsF_6]_{10}$	7.48	8.04	8.30	8.85

5,5′-H and 4,4′-H shift downfield and appear as multiplets because of the three-bond coupling to the neighboring protons on the same ring. Conversely, the resonances (doublets) for 3,3′-H are shifted upfield with respect to 3,3′-H of free bptz as a result of shielding by the pyridyl rings of the neighboring bptz units in the metallacycle.[73] Accordingly, $[Fe_4(bptz)_4(CH_3CN)_8][ClO_4]_8$ in CD_3CN exhibits four aromatic resonances in the ^{1}H NMR spectrum, in the same sequence and with very similar positions as those of $[Fe_4(bptz)_4(CH_3CN)_8][BF_4]_8$, i.e., δ 7.66, 8.02, 8.27, and 8.88 ppm ascribed to the 3,3′-, 5,5′-, 4,4′-, and 6,6′-H of the pyridyl rings, respectively (Table 1).

The ^{1}H NMR spectrum for the pentagon $[Fe_5(bptz)_5(CH_3CN)_{10}][SbF_6]_{10}$ in CD_3CN exhibits four sets of resonances in the aromatic region at δ 7.52, 8.07, 8.31, and 8.82 ppm assigned to the 3,3′-, 5,5′-, 4,4′-, and 6,6′-H of the pyridyl rings, respectively (Figure 6b; Table 1). Despite the fact that the resonances for $[Fe_5(bptz)_5(CH_3CN)_{10}][SbF_6]_{10}$ are similar to those of the aforementioned square polygons, which is not unexpected given the presence of the same metal ions and the similar chemical environments for the bptz protons in both polygons, the 3,3′- and 6,6′-H resonances for the pentagon are noticeably upfield-shifted as compared to the squares. Indeed, similar shifts are also observed in the ^{1}H NMR spectra of the pentagons $[Fe_5(bptz)_5(CH_3CN)_{10}][PF_6]_{10}$ and $[Fe_5(bptz)_5(CH_3CN)_{10}][AsF_6]_{10}$ in CD_3CN. The aromatic region for $[Fe_5(bptz)_5(CH_3CN)_{10}][PF_6]_{10}$ exhibits four sets

dx.doi.org/10.1021/ja3082473 | J. Am. Chem. Soc. 2013, 135, 3039−3055

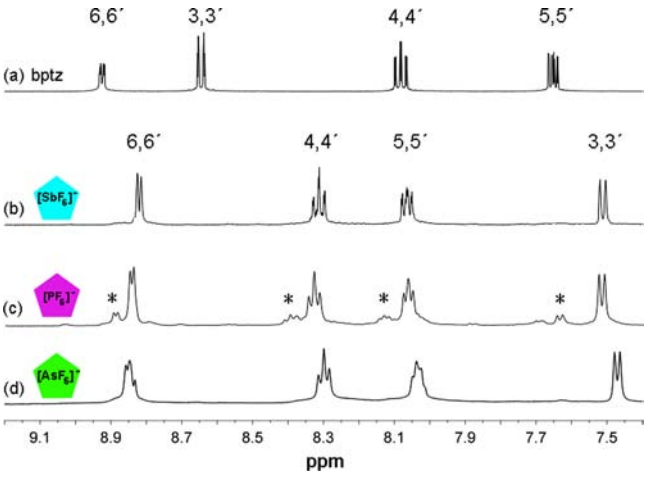

Figure 6. ^{1}H NMR spectra in CD_3CN of (a) free bptz, (b) $[Fe_5(bptz)_5(CH_3CN)_{10}][SbF_6]_{10}$, (c) $[Fe_5(bptz)_5(CH_3CN)_{10}][PF_6]_{10}$ (the resonances marked with an asterisk (*) are attributed to an open form of the metallacycle in solution, also contributing to the breadth of the closed metallacycle resonances), and (d) $[Fe_5(bptz)_5(CH_3CN)_{10}][AsF_6]_{10}$; the broad resonances in spectrum (d), despite excellent shimming, are attributed to paramagnetic impurities in the Fe(II) starting material.

of resonances at δ 7.52 (3,3′-H), 8.06 (5,5′-H), 8.33 (4,4′-H), and 8.84 (6,6′-H) (Figure 6c). Likewise, the ^{1}H NMR resonances for $[Fe_5(bptz)_5(CH_3CN)_{10}][AsF_6]_{10}$ appear at δ 7.48 (3,3′-H), 8.04 (5,5′-H), 8.30 (4,4′-H), and 8.85 (6,6′-H) (Figure 6d). Apparently, the resonances for protons 3,3′-H and 6,6′-H in the pentagonal cavities exhibit upfield shifts by $\Delta\delta \approx 0.10$ and 0.05 ppm, respectively, as compared to the corresponding protons in the squares (Table 1), because of the slightly more shielded environment in the former case; these upfield-shifted resonances assist in tracking the presence of the pentagonal versus the tetragonal metallacycles during the interconversion studies described in the ensuing section.

Interconversions of the Fe(II) Metallacycles Monitored by ^{1}H NMR Spectroscopy. The Fe(II) metallacycles with bptz are LS and thus diamagnetic,[91] which renders them amenable to ^{1}H NMR spectroscopic studies for characterization, as discussed earlier, as well as ideal candidates for ^{1}H NMR interconversion studies monitoring their self-assembly and relative stability in solution upon addition of the appropriate anions.

Conversion of $[Fe_5(bptz)_5(CH_3CN)_{10}][SbF_6]_{10}$ to $[Fe_4(bptz)_4(CH_3CN)_8][BF_4]_8$. A sample of $[Fe_5(bptz)_5(CH_3CN)_{10}][SbF_6]_{10}$ was dissolved in CD_3CN, and the ^{1}H NMR spectrum was recorded (Figure 7a). A 5-fold excess of $[n\text{-}Bu_4N][BF_4]$ was then added, and the sample was stirred for 1 h. No changes in the resonances of $[Fe_5(bptz)_5(CH_3CN)_{10}][SbF_6]_{10}$ were observed in the acquired ^{1}H NMR spectrum. Two separate additions of a 5-fold excess of $[n\text{-}Bu_4N][BF_4]$ to the sample were performed, and the mixture was stirred under nitrogen for 1 h and overnight in the two cases. The recorded ^{1}H NMR spectra are the same as that of the original $[Fe_5(bptz)_5(CH_3CN)_{10}][SbF_6]_{10}$ sample; that is, no conversion to the square took place. Subsequently, a fresh sample of $[Fe_5(bptz)_5(CH_3CN)_{10}][SbF_6]_{10}$ was dissolved in CD_3CN, and the solution was refluxed in the presence of a 25-fold excess of $[n\text{-}Bu_4N][BF_4]$ under nitrogen. The ^{1}H NMR spectrum of the solution was recorded at short time intervals; the onset of square formation was obvious at 1 h (Figure 7b), and at 2 h,

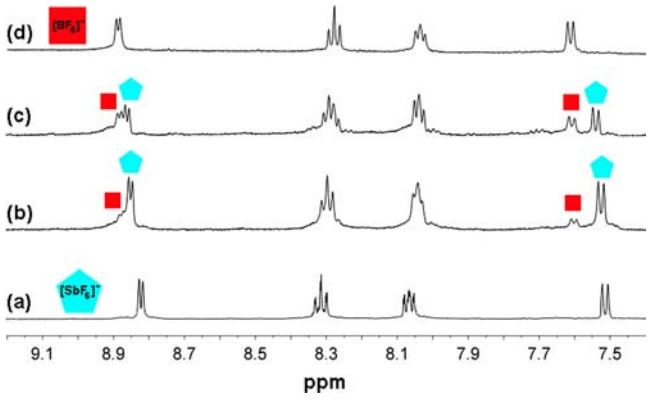

Figure 7. Conversion of $[Fe_5(bptz)_5(CH_3CN)_{10}][SbF_6]_{10}$ to $[Fe_4(bptz)_4(CH_3CN)_8][BF_4]_8$ monitored by NMR spectroscopy. ^{1}H NMR spectra in CD_3CN of (a) freshly dissolved $[Fe_5(bptz)_5(CH_3CN)_{10}][SbF_6]_{10}$; the reaction solution of $[Fe_5(bptz)_5(CH_3CN)_{10}][SbF_6]_{10}$ refluxed in the presence of a 25-fold excess of $[n\text{-}Bu_4N][BF_4]$ in CD_3CN for (b) 1, (c) 2, and (d) 4 h.

partial conversion of $[Fe_5(bptz)_5(CH_3CN)_{10}][SbF_6]_{10}$ to $[Fe_4(bptz)_4(CH_3CN)_8][BF_4]_8$ had occurred, as indicated by the presence of the square resonances for 3,3′-H and 6,6′-H at 7.61 and 8.89 ppm, respectively, in the spectrum (Figure 7c). Complete conversion of $[Fe_5(bptz)_5(CH_3CN)_{10}][SbF_6]_{10}$ to $[Fe_4(bptz)_4(CH_3CN)_8][BF_4]_8$ took place only after refluxing of the metallapentacycle for 4 h with a 25-fold excess of $[n\text{-}Bu_4N][BF_4]$, as indicated by the absence of the resonances for $[Fe_5(bptz)_5(CH_3CN)_{10}][SbF_6]_{10}$ at 7.52 (3,3′-H) and 8.82 (6,6′-H) ppm (Figure 7d).

Conversion of $[Fe_4(bptz)_4(CH_3CN)_8][BF_4]_8$ to $[Fe_5(bptz)_5(CH_3CN)_{10}][SbF_6]_{10}$. A sample of $[Fe_4(bptz)_4(CH_3CN)_8][BF_4]_8$ was dissolved in CD_3CN, and the ^{1}H NMR spectrum was recorded (Figure 8a). A 10-fold excess of $[n\text{-}Bu_4N][SbF_6]$ was added, and the sample was mildly heated to +45 °C for 20 h with no discernible changes in the ^{1}H NMR spectrum. A fresh sample of $[Fe_4(bptz)_4(CH_3CN)_8][BF_4]_8$ was dissolved in CD_3CN, and the solution was refluxed for 2 days in the presence of a 16-fold excess of $[n\text{-}Bu_4N][SbF_6]$ under

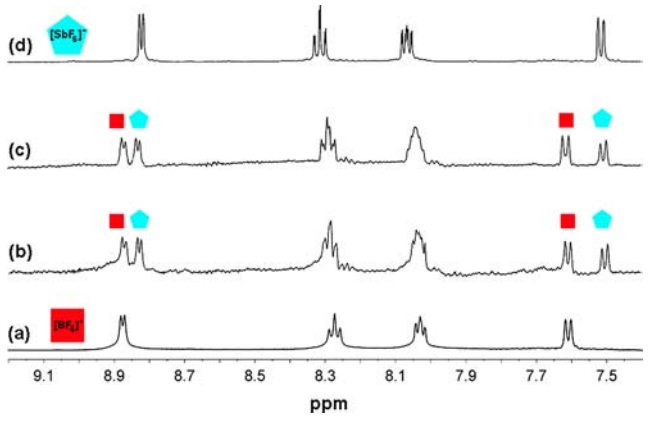

Figure 8. Conversion of $[Fe_4(bptz)_4(CH_3CN)_8][BF_4]_8$ to $[Fe_5(bptz)_5(CH_3CN)_{10}][SbF_6]_{10}$ monitored by NMR spectroscopy. ^{1}H NMR spectra in CD_3CN of (a) freshly dissolved $[Fe_4(bptz)_4(CH_3CN)_8][BF_4]_8$; the reaction solution of $[Fe_4(bptz)_4(CH_3CN)_8][BF_4]_8$ and a 16-fold excess of $[n\text{-}Bu_4N][SbF_6]$ refluxed for (b) 2 and (c) 4 days. (d) ^{1}H NMR spectrum of preformed $[Fe_5(bptz)_5(CH_3CN)_{10}][SbF_6]_{10}$ in CD_3CN.

dx.doi.org/10.1021/ja3082473 | J. Am. Chem. Soc. 2013, 135, 3039−3055

nitrogen. This resulted in a ~50:50% mixture of square/pentagon metallacycles (Figure 8b), as evidenced by the appearance of the upfield-shifted resonances at 7.52 (3,3′-H) and 8.82 (6,6′-H) ppm in the ^{1}H NMR spectrum (indicative of $[Fe_5(bptz)_5(CH_3CN)_{10}][SbF_6]_{10}$; Figure 8d). The same solution was refluxed for 2 additional days but no changes in the relative ratio of the pentagon to square resonances were observed in the ^{1}H NMR spectrum (Figure 8c).

An additional 10-fold excess of $[n\text{-}Bu_4N][SbF_6]$ was added (total 26-fold excess) to the previous sample, and the solution was refluxed for 2 additional days (total refluxing time of 6 days). No changes in the relative ratio of the pentagon to square resonances or the appearance of the ^{1}H NMR spectrum were noted as compared to Figure 8c. Finally, addition of a large excess of $[n\text{-}Bu_4N][BF_4]$ to the previous sample did not affect the equilibrium in favor of $[Fe_4(bptz)_4(CH_3CN)_8][BF_4]_8$, indicating that the system had reached thermodynamic equilibrium. Efforts to study the interconversion of $[Fe_4(bptz)_4(CH_3CN)_8][BF_4]_8$ to $[Fe_5(bptz)_5(CH_3CN)_{10}][PF_6]_{10}$ and vice versa, by ^{1}H NMR spectroscopy, were not successful because of the temperature sensitivity of $[Fe_5(bptz)_5(CH_3CN)_{10}][PF_6]_{10}$. Refluxing $[Fe_4(bptz)_4(CH_3CN)_8][BF_4]_8$ for 21 h or even mild heating for 2 h under N_2, in the presence of a 15-fold excess of $[n\text{-}Bu_4N][PF_6]$, resulted in precipitation of unidentifiable insoluble products.

Conversion of $[Fe_4(bptz)_4(CH_3CN)_8][BF_4]_8$ to $[Fe_5(bptz)_5(CH_3CN)_{10}][AsF_6]_{10}$. A sample of $[Fe_4(bptz)_4(CH_3CN)_8][BF_4]_8$ was dissolved in CD_3CN, and the ^{1}H NMR spectrum was recorded (Figure 9a). A 10-fold excess of

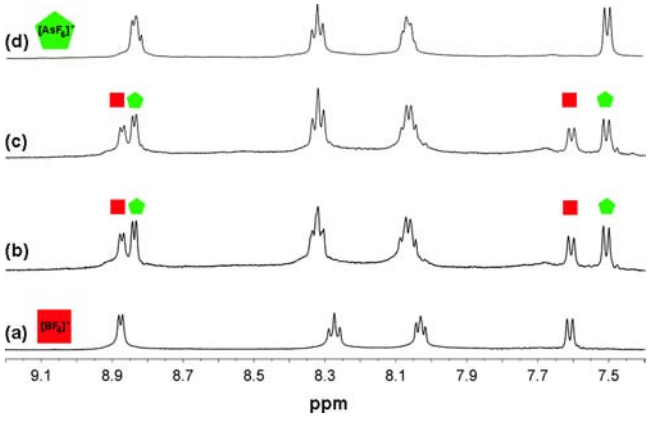

Figure 9. Conversion of $[Fe_4(bptz)_4(CH_3CN)_8][BF_4]_8$ to $[Fe_5(bptz)_5(CH_3CN)_{10}][AsF_6]_{10}$ monitored by ^{1}H NMR spectroscopy. ^{1}H NMR spectra in CD_3CN of (a) freshly dissolved $[Fe_4(bptz)_4(CH_3CN)_8][BF_4]_8$; the reaction solution of $[Fe_4(bptz)_4(CH_3CN)_8][BF_4]_8$ and a 15-fold excess of $KAsF_6$ in CD_3CN with stirring at +55 °C after (b) 12 and (c) 24 h. (d) ^{1}H NMR spectrum of preformed $[Fe_5(bptz)_5(CH_3CN)_{10}][AsF_6]_{10}$ in CD_3CN.

$KAsF_6$ was added, and the sample was mildly heated to +55 °C for 2 h with no changes occurring in the ^{1}H NMR spectrum. The addition of a 5-fold excess of $KAsF_6$ to the previous $[Fe_4(bptz)_4(CH_3CN)_8][BF_4]_8$ sample (total 15-fold excess of $KAsF_6$) with overnight stirring under N_2 at +55 °C, however, resulted in a ~44:56% mixture of the square $[Fe_4(bptz)_4(CH_3CN)_8][BF_4]_8$ and pentagon $[Fe_5(bptz)_5(CH_3CN)_{10}][AsF_6]_{10}$ metallacycles in solution (Figure 9b). The presence of $[Fe_5(bptz)_5(CH_3CN)_{10}][AsF_6]_{10}$ is indicated by the appearance of the upfield-shifted pentagon resonances for 3,3′-H and 6,6′-H at 7.49 and 8.84 ppm, respectively (Figure 9d). Heating the previous sample for an additional 12 h (total of 24 h) at +55 °C did not affect the equilibrium of the two metallacycles in solution (Figure 9c).

Anion-Template Studies of the Metallacycles. The anion-templated process was monitored by performing several small-scale reactions monitored by ^{1}H NMR spectroscopy. A solution of bptz in CD_3CN (3 mL) was added to a small equimolar quantity of $Fe(CF_3SO_3)_2$ in CD_3CN (3 mL), and the reaction mixture was stirred under a N_2 atmosphere for a short time. The ^{1}H NMR spectrum (Figure 10a) lacks the

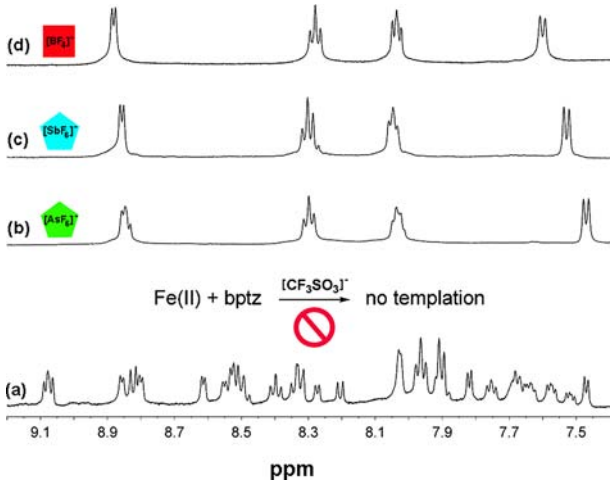

Figure 10. (a) ^{1}H NMR spectrum of the reaction mixture of $Fe(CF_3SO_3)_2$ and bptz in CD_3CN. ^{1}H NMR spectrum of the same solution as for trace (a) upon addition of (b) $KAsF_6$ (3-fold excess), (c) $[n\text{-}Bu_4N][SbF_6]$ (4-fold excess), and (d) $[n\text{-}Bu_4N][BF_4]$ (4-fold excess).

characteristic features of the aforementioned highly symmetric polygons (Figures 5b and 6b–d) and hints at the formation of oligomeric mixtures of Fe(II)/bptz moieties in the presence of $[CF_3SO_3]^-$ anions, thereby indicating that the latter are non-templating anions. The initial solution of $Fe(CF_3SO_3)_2$ with bptz in CD_3CN (Figure 10a) was subsequently separated into three 2 mL portions; an excess amount of $KAsF_6$ (3-fold), $[n\text{-}Bu_4N][SbF_6]$ (4-fold), or $[n\text{-}Bu_4N][BF_4]$ (4-fold) was added to each portion and the ^{1}H NMR spectra were recorded (Figure 10b–d, respectively). The ^{1}H NMR data are in accord with the spectra of the preformed polygons $[Fe_5(bptz)_5(CH_3CN)_{10}][AsF_6]_{10}$, $[Fe_5(bptz)_5(CH_3CN)_{10}][SbF_6]_{10}$, and $[Fe_4(bptz)_4(CH_3CN)_8][BF_4]_8$, respectively (Figures 6d, 6b, and 5b, respectively), thus providing incontrovertible evidence for an anion templation effect occurring in the presence of suitable templating anions, namely, $[AsF_6]^-$, $[SbF_6]^-$, or $[BF_4]^-$. Reactions of Zn(II) with bptz were also found to be under templation control, thus further underscoring the pivotal role of the anion in stabilizing a specific metallacycle (Figures S10 and S11). To our knowledge, anion-based templation was verified in solution by ^{1}H NMR spectroscopy for two Co(II) tetrahedral cages.[22,25]

^{19}F NMR Spectroscopy of the Fe(II) Metallacycles in Solution. ^{19}F NMR spectra in solution were acquired for $[Fe_4(bptz)_4(CH_3CN)_8][BF_4]_8$, $[Fe_5(bptz)_5(CH_3CN)_{10}][PF_6]_{10}$, $[Fe_5(bptz)_5(CH_3CN)_{10}][SbF_6]_{10}$, and $[Zn_4(bptz)_4(CH_3CN)_8][BF_4]_8$.

$[Fe_4(bptz)_4(CH_3CN)_8][BF_4]_8$. The ^{19}F NMR spectra of $[Fe_4(bptz)_4(CH_3CN)_8][BF_4]_8$ in CD_3CN between +20 and

dx.doi.org/10.1021/ja3082473 | J. Am. Chem. Soc. 2013, 135, 3039–3055

−40 °C exhibit one resonance at $\delta \approx -150$ ppm (Figure S12), which is ascribed to the free $[BF_4]^-$ ions.[73,92,93] Despite extensive experimental efforts, it was not possible to observe a second ^{19}F NMR resonance of lower intensity for the encapsulated $[BF_4]^-$ ions, by variable-temperature (VT) experiments.[88,92−94] The resonance at $\delta \approx -150$ ppm, however, exhibits considerable broadening with increasing temperature in the range between −40 and +20 °C, an indication of rapid $[BF_4]^-$ anion exchange on the time scale of the NMR experiment.[93,95−97] The inability to observe the ^{19}F NMR resonance corresponding to the $[BF_4]^-$ anions in the cavity of the polygons can also be attributed to broadening due to the paramagnetic contribution from a small percentage of HS Fe(II) atoms,[91,97] contributing to faster relaxation of the ^{19}F nuclei.

$[Fe_5(bptz)_5(CH_3CN)_{10}][PF_6]_{10}$. The ^{19}F NMR spectrum of $[n\text{-}Bu_4N][PF_6]$ in CD_3CN at +22 °C exhibits a doublet at $\delta \approx -71$ ppm $[J(^{19}F-^{31}P) = 710$ Hz$]$, assigned to free $[PF_6]^-$ ions. Likewise, the ^{19}F NMR spectrum of $[Fe_5(bptz)_5(CH_3CN)_{10}][PF_6]_{10}$ in CD_3CN at +22 °C exhibits a doublet at $\delta \approx -71$ ppm $[J(^{19}F-^{31}P) = 710$ Hz$]$ due to the free $[PF_6]^-$ ions.[45,95,98] At −40 °C, however, a second substantially upfield-shifted ^{19}F doublet resonance of lower intensity appears at $\delta \approx -180$ ppm (Figure S13 inset), which is ascribed to the encapsulated $[PF_6]^-$ ions in the cavity of $[Fe_5(bptz)_5(CH_3CN)_{10}][PF_6]_{10}$.[94] Possible factors contributing to the substantial upfield shift of the NMR resonance for the encapsulated $[PF_6]^-$ anions in $[Fe_5(bptz)_5(CH_3CN)_{10}][PF_6]_{10}$, as compared to the corresponding free anions, are detailed in the Supporting Information. It is important to note that the lower-intensity ^{19}F NMR resonance at $\delta \approx -180$ ppm is reproducible in several different batches of $[Fe_5(bptz)_5(CH_3CN)_{10}][PF_6]_{10}$ but is clearly absent from the ^{19}F NMR spectra of the starting materials $TlPF_6$ and $[Fe(CH_3CN)_6][PF_6]_2$ used to prepare $[Fe_5(bptz)_5(CH_3CN)_{10}][PF_6]_{10}$; this fact eliminates the possibility of impurities giving rise to the resonance. The ^{19}F NMR spectrum of $[Fe_5(bptz)_5(CH_3CN)_{10}][SbF_6]_{10}$ in solution is discussed in the Supporting Information (see also Figure S14).

The encapsulated $[PF_6]^-$ anions are in dynamic exchange with the free anions in solution,[93,95−98] as evidenced by the broadening of both the ^{19}F NMR resonances observed in the spectra of $[Fe_5(bptz)_5(CH_3CN)_{10}][PF_6]_{10}$, upon lowering the temperature to −40 °C. The population difference of the two types of $[PF_6]^-$ anions and the line-width analyses of the ^{19}F NMR resonances (determined as ∼97 and ∼150 Hz for the free and encapsulated anions, respectively) permit the calculation of the $[PF_6]^-$ anion-exchange rate, which is $k_{exc(PF_6)} = 166(16)$ s^{-1} at −40 °C; this value corresponds to an activation energy of encapsulation $\Delta G^{\ddagger}_{233K(PF_6)} = 46(4)$ kJ/mol at 233 K for the $[PF_6]^-$ anions.

$[Zn_4(bptz)_4(CH_3CN)_8][BF_4]_8$. As previously reported, the spectra of $[Zn_4(bptz)_4(CH_3CN)_8][BF_4]_8$ in CD_3CN exhibit two ^{19}F NMR resonances at $\delta \approx -151$ and −144 ppm, between −10 and −35 °C, ascribed to free and encapsulated $[BF_4]^-$ ions, respectively.[73] The low intensity resonance at −144 ppm is downfield-shifted by $\Delta\delta \approx 6.0$ ppm relative to that of free $[BF_4]^-$ ions. This chemical shift difference, characteristic of the encapsulated $[BF_4]^-$ ions interacting with the metallacyclophane edges, is significant and compares well with the $\Delta\delta(^1H)$ values observed for strong hydrogen bonds or the $\Delta\delta(^{19}F)$ values for various intermolecular noncovalent interactions.[99] The encapsulated $[BF_4]^-$ anions are in dynamic exchange with the free anions in solution,[98] as evidenced by a broadening of the ^{19}F NMR resonances in the spectra of $[Zn_4(bptz)_4(CH_3CN)_8][BF_4]_8$ upon lowering the temperature (the encapsulated anion ^{19}F resonance line width increases from ∼58 to ∼160 Hz upon cooling from −10 to −35 °C). From the analyses of the ^{19}F NMR resonances, the $[BF_4]^-$ anion-exchange rate for $[Zn_4(bptz)_4(CH_3CN)_8][BF_4]_8$ was calculated to be $k_{exc(BF_4)} = 140(14)$ s^{-1} at 238 K, yielding an activation energy of encapsulation $\Delta G^{\ddagger}_{238K(BF_4)} = 48(4)$ kJ/mol for the $[BF_4]^-$ anions.

Solid-State MAS ^{19}F NMR Spectroscopy[100] of the Metallacycles. *$[\{Fe_4(bptz)_4(CH_3CN)_8\}\subset BF_4][BF_4]_7$.* The room-temperature ^{19}F MAS NMR spectrum of a solid sample of $[\{Fe_4(bptz)_4(CH_3CN)_8\}\subset BF_4][BF_4]_7$, spinning at a rate of 12 kHz, exhibits a resonance, shifted downfield by ∼10 ppm relative to that of solid $NaBF_4$ (Figures S15a and S16a). The ^{19}F MAS NMR resonance for $[\{Fe_4(bptz)_4(CH_3CN)_8\}\subset BF_4][BF_4]_7$ is significantly broadened ($\Delta\nu \approx 2400$ Hz) as compared to $NaBF_4$ and nonsymmetrical relative to a maximum (Figure S16a). An applied procedure of line narrowing to this broad resonance results in resolution of three overlapping resonances with chemical shifts $\delta \approx 13.1$, 11.4, and 9.7 ppm (Figure S16b) and relative intensities 1:3:4, which indicate that there are three different types of $[BF_4]^-$ anions in $[\{Fe_4(bptz)_4(CH_3CN)_8\}\subset BF_4][BF_4]_7$ in the solid state.

$[\{Zn_4(bptz)_4(CH_3CN)_8\}\subset BF_4][BF_4]_7$.[73] The room-temperature ^{19}F MAS NMR spectrum of solid $[Zn_4(bptz)_4(CH_3CN)_8][BF_4]_8$, spinning at a rate of 10 kHz, exhibits two resonances with isotropic chemical shifts $\delta \approx 12.0$ and 9.5 ppm (Figure S15d). Both resonances are downfield-shifted relative to free $[BF_4]^-$ ions in solution (Figure S15b), they exhibit Lorentzian shapes, and the low-field line is more broadened. Because MAS NMR experiments average heteronuclear coupling,[100] the more broadened low-field resonance is ascribed to the presence of two unresolved lines. This is confirmed by the partially relaxed ^{19}F NMR spectrum collected by inversion−recovery experiments for $[Zn_4(bptz)_4(CH_3CN)_8][BF_4]_8$ wherein it is clear that three resonances are present at $\delta \approx 12.4$, 11.1, and 9.5 ppm (Figure S15c).

$[\{Fe_5(bptz)_5(CH_3CN)_{10}\}\subset 2SbF_6][SbF_6]_8$. The room-temperature ^{19}F MAS NMR spectrum of $[Fe_5(bptz)_5(CH_3CN)_{10}][SbF_6]_{10}$, spinning at a rate of 12 kHz, shows a resonance centered at $\delta \approx 40.4$ ppm (Figure S17b), which is shifted downfield by $\Delta\delta \approx 18$ ppm as compared to solid $NaSbF_6$ (centered at ∼22.5 ppm relative to solid $NaBF_4$; Figures S15a and S17a). By applying a procedure of mathematical line narrowing, the solid-state ^{19}F NMR resonance of $[Fe_5(bptz)_5(CH_3CN)_{10}][SbF_6]_{10}$ is transformed to the pattern shown in Figure S17c, in which at least 20 overlapping lines are well resolved. Within this multiplet, one can distinguish a sextet with a coupling constant of $^1J_1(^{19}F-^{121}Sb) \approx 1940-1950$ Hz, which is comparable to $^1J(^{19}F-^{121}Sb)$ for free $[SbF_6]^-$ ions in CD_3CN (vide supra; Figure S14), as well as an octet with a coupling constant of $^1J(^{19}F-^{123}Sb) \approx 1033$ Hz. Aside from these features, however, the lines in the multiplet show additional splittings of ∼630 and ∼1230 Hz, which cannot be attributed to $^1J(^{19}F-^{121,123}Sb)$ spin−spin couplings. Because the isotopic shift ($^{19}F-^{121,123}Sb$) is not detectable in the solid-state NMR spectra, the complex ^{19}F NMR pattern in Figure S17c can be assigned to three types of inequivalent $[SbF_6]^-$ ions being

dx.doi.org/10.1021/ja3082473 | J. Am. Chem. Soc. 2013, 135, 3039−3055

present in $[\{Fe_5(bptz)_5(CH_3CN)_{10}\}\subset 2SbF_6][SbF_6]_8$ with relative chemical shifts $\delta \approx 0.0$, 1.6, and 3.9 ppm. A complete analysis of the pattern is not possible, but nonetheless, a pattern very similar to that in Figure S17c can be generated on the basis of three experimentally observed ^{19}F NMR resonances for solid $NaSbF_6$ (with integral intensity ratios ~1:1.6:2.5 or 2:3:5) and practically the same chemical shift differences (Figure S18), thus corresponding to chemical shifts of $\delta \approx 43.3$, 40.0, and 39.4 ppm in Figure S17c.

Electrochemistry. The molecular square $[Fe_4(bptz)_4(CH_3CN)_8][BF_4]_8$ in CH_3CN (0.15 M $[n\text{-}Bu_4N][BF_4]$) exhibits four consecutive reversible Fe(II)-based oxidations at $E_{1/2}$ = −0.094, +0.047, +0.32, and +0.52 V (Figure 11), in addition to the irreversible bptz reduction feature at −1.07 V. The first two metal-centered Fe(II)/Fe(III) oxidation events closely overlap, a fact that is attributed to redox events occurring at the Fe(II) sites occupying opposing vertices in the square metallacycle. It thus becomes more difficult for the remaining Fe(II) ions, which are adjacent to the Fe(III) ions, to be oxidized, thereby leading to an increase in their oxidation potentials.

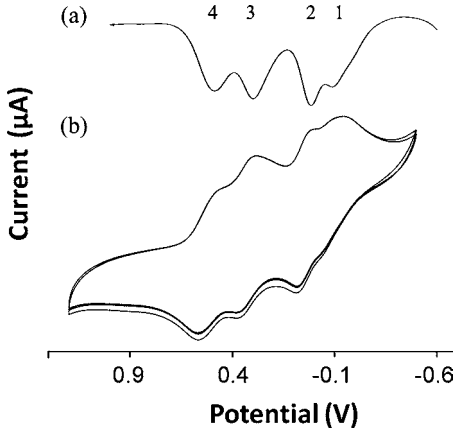

Figure 11. (a) Differential pulse voltammetry (DPV) and (b) cyclic voltammetry (CV) of $[Fe_4(bptz)_4(CH_3CN)_8][BF_4]_8$ versus Ag/AgCl in CH_3CN (in 0.15 M $[n\text{-}Bu_4N][BF_4]$ supporting electrolyte) with a Pt working electrode at a scan rate of 0.2 V/s at 25 °C.

The Fe(II)/bptz metallapentacycles exhibit similar electrochemical behavior, which involves oxidation of the Fe(II) ions at non-neighboring vertices of the polygons at low potentials, with minimal influence from the remaining Fe(II) ions, which are subsequently oxidized at higher potentials (Table 2). The cyclic voltammagram for $[Fe_5(bptz)_5(CH_3CN)_{10}][SbF_6]_{10}$ in CH_3CN exhibits two Fe(II)/Fe(III) nearly overlapping reversible oxidation couples that occur at very similar $E_{1/2}$ values of −0.027 and +0.034 V followed by two clearly resolved events at higher potentials (+0.37, +0.56 V; Figure S19). In the case of $[Fe_5(bptz)_{10}(CH_3CN)_{10}][AsF_6]_{10}$, there are closely spaced Fe(II)/Fe(III) events whose reversibility is less apparent than in the previously described cases (Figure S20; Table 2). Additionally, the metallacycle $[Fe_5(bptz)_{10}(CH_3CN)_{10}][PF_6]_{10}$ exhibits a few reversible Fe(II)/Fe(III) oxidation steps followed by a quasi-reversible oxidation at a higher potential (Figure S21), which is not surprising, as we have established by NMR spectroscopy that it is less stable than the pentagonal metallacycles with other templating anions. The irreversible reduction feature for the bptz ligand in $[Fe_5(bptz)_{10}(CH_3CN)_{10}][PF_6]_{10}$ occurs at −1.01 V versus Ag/AgCl and at more negative potentials for $[Fe_5(bptz)_5(CH_3CN)_{10}][SbF_6]_{10}$ and $[Fe_5(bptz)_{10}(CH_3CN)_{10}][AsF_6]_{10}$ (−1.22 and −1.48 V, respectively), thus also confirming the higher redox stabilities of $[Fe_5(bptz)_5(CH_3CN)_{10}][SbF_6]_{10}$ and $[Fe_5(bptz)_{10}(CH_3CN)_{10}][AsF_6]_{10}$ versus $[Fe_5(bptz)_{10}(CH_3CN)_{10}][PF_6]_{10}$.

Stability of the Fe(II) Metallacycles in Solution Evidenced by Cyclic Voltammetric Studies. The Fe(II)/bptz polygons explored herein exhibit rich electrochemical behavior with several metal-centered reversible sequential Fe(II)/Fe(III) oxidation processes for each (Figures 11 and S19−S21; Table 2).

The remarkable separation range of ~600−650 mV between the oxidation processes for each Fe(II) metallacycle under discussion (Table 2) indicates considerable electronic communication between the Fe(II) centers mediated by the tetrazine rings.[101] More importantly, the electrochemical studies support the remarkable stability of the intact polygons $[Fe_4(bptz)_4(CH_3CN)_8][BF_4]_8$, $[Fe_5(bptz)_5(CH_3CN)_{10}][SbF_6]_{10}$, $[Fe_5(bptz)_5(CH_3CN)_{10}][AsF_6]_{10}$, and to a lesser extent $[Fe_5(bptz)_5(CH_3CN)_{10}][PF_6]_{10}$ in solution. In contrast to the reduction of the bptz ligand in the polygons being irreversible, the reduction of free bptz is reversible.[102] The irreversibility of the ligand-based reductions in the polygons indicates destruction of the metallacycles, which can be attributed to their destabilization with decreasing π-acidity of the central rings, thereby weakening the anion−π interactions with the encapsulated anions. Conversely, oxidation of the metal centers increases the π-acidity of the rings and thus the favorable anion−π contacts between the encapsulated anions and the π-acidic rings, thereby granting exceptional stability to the metallacycles. It is also noteworthy that the reduction for the free bptz ligand is more facile than that for the metallacycles (Table 2), indicating more electron-rich bptz moieties in the polygons, which is attributed to the anion−π contacts with the encapsulated anions.[103] In the absence of anion−π contacts, however, the reduction of the bound bptz ligand would be

Table 2. Electrochemical Data[a] for Fe(II) Metallacycles with bptz

	$E_{1/2}$(ox) (V)				
complex	I	II	III	IV	E_{red}(bptz) (V)
$[Fe_4(bptz)_4(CH_3CN)_8][BF_4]_8$[b]	−0.094[e]	+0.047[e]	+0.32[e]	+0.52[e]	−1.07[g]
$[Fe_5(bptz)_5(CH_3CN)_{10}][SbF_6]_{10}$[c]	−0.027[e]	+0.034[e]	+0.37[e]	+0.56[e]	−1.22[g]
$[Fe_5(bptz)_5(CH_3CN)_{10}][AsF_6]_{10}$[d]	−0.090[e]	+0.040[e]	+0.34[e]	+0.58[e]	−1.48[g]
$[Fe_5(bptz)_5(CH_3CN)_{10}][PF_6]_{10}$[d]	−0.085[e]	+0.039[e]	+0.32[e]	+0.55[f]	−1.01[g]
bptz[d]					−0.72[e]

[a]Data collected in CH_3CN versus Ag/AgCl at 25 °C. [b]Supporting electrolyte 0.15 M $[n\text{-}Bu_4N][BF_4]$. [c]Supporting electrolyte 0.20 M $[n\text{-}Bu_4N][SbF_6]$. [d]Supporting electrolyte 0.15 M $[n\text{-}Bu_4N][PF_6]$. [e]Reversible. [f]Quasi-reversible. [g]Irreversible.

dx.doi.org/10.1021/ja3082473 | J. Am. Chem. Soc. 2013, 135, 3039−3055

expected to occur at less negative potentials due to the coordination of the cationic metal atoms. In short, the findings from the electrochemical behavior of the metallacycles further emphasize the presence and importance of the anion−π interactions in stabilizing the assemblies in solution.

Computational Studies. In the DFT studies, the interactions for the geometry-optimized single- and double-ring complexes between the 3,6-difluoro and 3,6-dicyano derivatives of tetrazine and the $[BF_4]^-$ or $[PF_6]^-$ anions were evaluated by DFT methods; the results are collected in Table 3 and depicted in Figures 12, 13 and Figures S22, S23). The tetrazine derivatives were used to avoid hydrogen-bond formation with the F atoms of the anions without imposing symmetry restraints on the systems, as well as to increase the π-acidity of the tetrazine ring. As indicated in Figure S24, the dicyanotetrazine ring is more π-acidic than the difluoro derivative, and both molecules are amenable to anion−π interactions.

Table 3. Equilibrium Distances $R_{F\cdots C(tetrazine)}$ (Å) and Binding Energies (kcal mol^{-1}) for the Geometry-Optimized Complexes $C_2N_4R_2\cdots[X]^-$ and $C_2N_4R_2\cdots[X]^-\cdots C_2N_4R_2$ (R = F, CN; $[X]^-$ = $[BF_4]^-$, $[PF_6]^-$) at the B3LYP/6-31+G(d) Level of Theory

complex	$R_{F\cdots C(tetrazine)}$ (Å)	E (kcal mol^{-1})
$C_2N_4F_2\cdots[BF_4]^-$	2.69[a]	−12.3
$C_2N_4(CN)_2\cdots[BF_4]^-$	2.63[a]	−18.4
$C_2N_4F_2\cdots[PF_6]^-$	2.88	−9.6
	2.78	
$C_2N_4(CN)_2\cdots[PF_6]^-$	2.80	−14.6
	2.70	
$C_2N_4F_2\cdots[BF_4]^-\cdots C_2N_4F_2$	2.74[a,b]	−23.0
$C_2N_4(CN)_2\cdots[BF_4]^-\cdots C_2N_4(CN)_2$	2.71[a,b]	−33.2
$C_2N_4F_2\cdots[PF_6]^-\cdots C_2N_4F_2$	2.80[b]	−18.1
	2.86[b]	
$C_2N_4(CN)_2\cdots[PF_6]^-\cdots C_2N_4(CN)_2$	2.77[b]	−26.7
	2.83[b]	

[a]Two contacts per ring. [b]$F\cdots C_{tetrazine}$ distances to two opposing rings are equal.

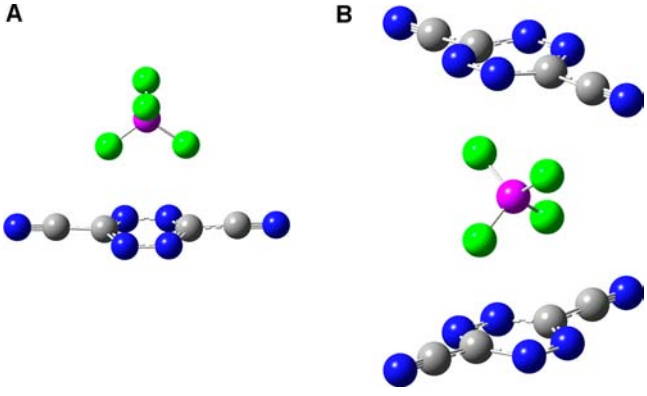

Figure 12. Side view of ball-and-stick representations for the geometry-optimized complexes at the B3LYP/6-31+G(d) level of theory: (A) $C_2N_4(CN)_2\cdots[BF_4]^-$ and (B) $C_2N_4(CN)_2\cdots[BF_4]^-\cdots C_2N_4(CN)_2$. Atom colors: C, gray; N, blue; F, green; B, purple.

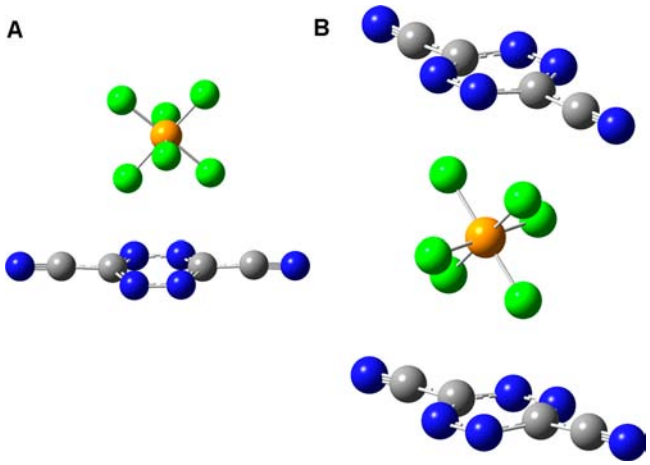

Figure 13. Side view of ball-and-stick representations for the geometry-optimized complexes at the B3LYP/6-31+G(d) level of theory: (A) $C_2N_4(CN)_2\cdots[PF_6]^-$ and (B) $C_2N_4(CN)_2\cdots[PF_6]^-\cdots C_2N_4(CN)_2$. Atom colors: C, gray; N, blue; F, green; P, orange.

We performed the calculations for the geometry-optimized complexes at the B3LYP/6-31+G(d) level of theory, which yields smaller binding energies and longer distances $R_{F\cdots C(tetrazine)}$ than the MP2 level, facts established in comparative studies for relevant systems with this type of interactions.[37,104,105] This is also corroborated by a comparison of our results with those for the complex of 3,6-difluorotetrazine with $[BF_4]^-$ ions previously studied at the MP2/6-31++G** level of theory.[106] Nonetheless, the B3LYP/6-31+G(d) level results have been shown to provide good qualitative trends for anion−π interactions (as compared to the MP2 level)[37] and proved to be in good agreement with our experimental results (vide infra). In the single-ring complexes, the distances $R_{F\cdots C(tetrazine)}$ to the polyatomic anions $[BF_4]^-$ or $[PF_6]^-$ are considerably shorter than $\sum R_{vdW}$ F···C (3.17 Å) and the energies are negative (Table 3), thus indicating that the interactions between the substituted tetrazine rings and the anions are favorable.[32,33] As expected, the energy values are more negative and the $R_{F\cdots C(tetrazine)}$ distances are shorter for both rings with $[BF_4]^-$ as compared to the respective values for the larger $[PF_6]^-$ anion (Table 3; the same trends were observed for trifluorotriazine,[107a] tetrazine[107b] and other systems with halides[67b] studied at the MP2/6-31++G** and B3LYP/6-31+G(d,p) levels of theory, respectively). Moreover, because of the higher π-acidity of dicyanotetrazine as compared to the difluoro derivative (Figure S24), the binding energies are more negative, indicating stronger interactions, for the former complexes as compared to the latter (Table 3).

In the geometry-optimized single-ring complexes, it is clear that there is a symmetric positioning of the $[BF_4]^-$ or $[PF_6]^-$ anions over the ring centroids of 3,6-dicyanotetrazine (Figures 12A and 13A) or 3,6-difluorotetrazine (Figures S22A and S23A), and that each complex possesses a C_2 symmetry axis perpendicular to the ring plane. For both anions, two anion F atoms are pointed toward the two C atoms of the tetrazine moieties, which are the more π-acidic regions of the ring, and engage in two directional F···C anion−π interactions; moreover, the two F atoms of $[BF_4]^-$ are equidistant (or within 0.10 Å for $[PF_6]^-$) from the tetrazine C atoms (Table 3). The same positioning of $[BF_4]^-$ over the ring was found for 3,6-difluorotetrazine studied at the MP2/6-31++G** level of theory.[106] Also, a symmetric positioning of the anions was

dx.doi.org/10.1021/ja3082473 | J. Am. Chem. Soc. 2013, 135, 3039−3055

observed for the trifluorotriazine complexes with $[BF_4]^-$ and $[PF_6]^-$ studied at the MP2/6-31++G** level of theory, with preference for the establishment of three short F···C anion contacts with the trifluorotriazine carbon atoms.[107a]

To better assess the positioning and short contacts of the encapsulated polyatomic anions $[BF_4]^-$ and $[SbF_6]^-$ in the metallacycles previously studied[71−73] as well as in this work, we also undertook calculations of the model binary adducts $C_2N_4R_2\cdots[X]^-\cdots C_2N_4R_2$ (R = F, CN; $[X]^-$ = $[BF_4]^-$ or $[PF_6]^-$ as an exemplary octahedral anion). The energy values and the $R_{F\cdots C(tetrazine)}$ distances in the $C_2N_4R_2\cdots[X]^-\cdots C_2N_4R_2$ complexes exhibit similar trends with respect to the arene substituents as in $C_2N_4R_2\cdots[X]^-$, namely, greater binding energies and shorter distances for the dicyano as compared to the difluoro derivative of tetrazine (Table 3).

The binary complexes $C_2N_4R_2\cdots[BF_4]^-\cdots C_2N_4R_2$ (R = F, CN) display optimized geometries in which the two tetrazine moieties are rotated by 90° with respect to each other, an orientation that maximizes the number of F···$C_{tetrazine}$ contacts of the $[BF_4]^-$ anion with both rings and serves to accommodate the tetrahedral geometry of the anion (Figures 12B and S22B). In the $C_2N_4R_2\cdots[BF_4]^-\cdots C_2N_4R_2$ complexes, the four F atoms of the $[BF_4]^-$ anion are directly positioned toward the four carbon atoms (two per ring; the C atoms correspond to the more π-acidic regions) of the two rings, with the $R_{F\cdots C(tetrazine)}$ contacts being ∼0.40 Å shorter than $\sum R_{vdW}$ F···C (2.74 and 2.71 Å for R = F and CN, respectively; Table 3), but slightly longer than those in the corresponding single-ring $C_2N_4R_2\cdots[BF_4]^-$ complexes (2.69 and 2.63 Å for R = F and CN, respectively). These findings with respect to the distances resemble the results of other comparable systems with two rings and one anion.[67b]

The binary adducts $C_2N_4R_2\cdots[PF_6]^-\cdots C_2N_4R_2$ (R = F, CN) display optimized geometries in which the substituted tetrazine moieties maximize the F···C contacts with the $[PF_6]^-$ anions (two per ring; Figures 13B and S23B). In the $C_2N_4R_2\cdots[PF_6]^-\cdots C_2N_4R_2$ complexes, the two tetrazine rings are eclipsed, as opposed to the 90° angle between the ring substituents in the binary complexes with the $[BF_4]^-$ anions; this is attributed to the octahedral geometry of the $[PF_6]^-$ anion, which allows two F···$C_{tetrazine}$ close contacts with each of the two eclipsed tetrazine rings. Four fluorine atoms of the $[PF_6]^-$ anion are directed toward the four carbon atoms of the two opposing rings (these are the more π-acidic regions of the rings). The $R_{F\cdots C(tetrazine)}$ contacts in the double-ring complexes with $[PF_6]^-$ anions are by ∼0.37 Å shorter than $\sum R_{vdW}$ F···C (average values 2.83 and 2.80 Å for R = F and CN, respectively; Table 3), and as in the case of the $[BF_4]^-$ anions, they are slightly longer than those in the corresponding single-ring complexes $C_2N_4R_2\cdots[PF_6]^-$ (average values 2.81 and 2.75 Å for R = F and CN, respectively).

For both the $[BF_4]^-$ and $[PF_6]^-$ anions, the $R_{F\cdots C(tetrazine)}$ distances for the binary systems are essentially insensitive to the complex stoichiometry, as previously reported by Deyà et al.[108] for monoatomic anions with halide derivatives of 1,3,5-triazine. Additionally, the binding energies of the binary systems with $[BF_4]^-$ or $[PF_6]^-$ anions are favorable and approximately twice the binding energies of the respective complexes with only one tetrazine ring (Table 3), in agreement with the studies showing that anion−π interactions are additive in π-acidic systems with monoatomic anions.[67b,108]

DISCUSSION

Anion−π Contacts of the Fe(II) Metallacycles in the Solid State. Tetrazine is a nitrogen-rich π-acidic aromatic heterocycle, which poises it to engage in anion−π interactions.[51b,73,74] Moreover, recent theoretical studies indicated that the anion−π binding ability of the tetrazine ring is enhanced by multiple N coordination to metal ions.[51b] Thus, the Fe(II) polygons, with the bptz moieties spanning their edges and providing a π-acidic interior, are excellent candidates to engage in anion−π contacts with the encapsulated anions, as previously shown for the Ni(II) and Zn(II) congeners,[71−73] as well as for other relevant π-acidic cavities involving metal ions.[43,45,47] The Fe(II) metallacycles **1** and **2** are structurally similar to the Ni(II) congeners $[Ni_4(bptz)_4(CH_3CN)_8][BF_4]_8$[71,73] and $[Ni_5(bptz)_5(CH_3CN)_{10}][SbF_6]_{10}$,[72,73] respectively. The Fe(II) metallacycle cavities of **1** and **2** are smaller, however, because there is a significant contraction in the M(II)···M(II) vertex separations in both Fe(II) polygons as compared to the corresponding Ni(II) congeners; this is due to population of the e_g orbitals on going from the LS Fe(II) to the HS Ni(II) congeners (for the squares, ∼6.5 Å for Fe(II) versus ∼6.9 Å for Ni(II); for the pentagons, ∼6.4 Å for Fe(II) versus ∼6.7 Å for Ni(II)). The metallacycle $[\{Fe_4(bptz)_4(CH_3CN)_8\}\subset BF_4]^{7+}$ has the smallest cavity from the polygon series investigated to date. Both Fe(II) polygons exhibit higher than the statistically favored (55%) cavity occupancy by the guest anions[109] (void cavity volume calculations were carried out on the crystal structures of $[Fe_4(bptz)_4(CH_3CN)_8]^{8+}$ and $[Fe_5(bptz)_5(CH_3CN)_{10}]^{10+}$);[110−113] this is usually attained when intermolecular host−guest interactions are present[90,114] (anion−π host−guest interactions in the case of the Fe(II) polygons). In both **1** and **2**, the cations with π-acidic interiors are excellent hosts for the encapsulated anions. Indeed, a tightly packed $[BF_4]^-$ anion resides in the cavity of **1** (Figure 2) and is equally disordered over two positions such as to allow the F atoms of the $[BF_4]^-$ anion to maximize contacts with the two sets of opposing tetrazine rings (Figure 3). The encapsulated $[BF_4]^-$ anion exhibits the ideal tetrahedral geometry to interact with the edges of the square and engages in four short F···C contacts for every anion position of disorder; the anion is poised in a manner to establish two close F···C directional contacts with each tetrazine ring, with two F atoms lying over the two electropositive C atoms of each central ring at an average distance of F···C ≈ 2.84 Å (Figure 3).

The DFT calculations are in excellent agreement with the X-ray structural data with respect to the positioning of the anions as well as the predicted distances in the optimized binary adducts $C_2N_4R_2\cdots[BF_4]^-\cdots C_2N_4R_2$ (R = F, CN). In these complexes, the two tetrazine moieties are rotated by 90° with respect to one another, and the four F atoms of the tetrahedral $[BF_4]^-$ anion are directed at the four carbon atoms that correspond to the more π-acidic regions of the two rings (two per ring; Figures 12B and S22B). As detailed in the preceding paragraph, the same positioning of the $[BF_4]^-$ anion with respect to the opposing rings is encountered in $[\{Fe_4(bptz)_4(CH_3CN)_8\}\subset BF_4]^{7+}$ with the only difference being that, in the crystal structure, the opposing tetrazine moieties (and thus the bptz ligands) are rotated by 60° only (instead of 90° in the optimized model with untethered tetrazine rings) with respect to one another because of the structural constraints imposed due to chelation to the metal centers. Despite this fact, the computationally derived F···$C_{tetrazine}$ distance (2.71 Å) in the

dx.doi.org/10.1021/ja3082473 | J. Am. Chem. Soc. 2013, 135, 3039−3055

geometry-optimized binary complex $C_2N_4(CN)_2\cdots[BF_4]^-\cdots C_2N_4(CN)_2$ in the gas phase is only slightly shorter than the crystallographically determined F···$C_{tetrazine}$ distances for $[Fe_4(bptz)_4(CH_3CN)_8][BF_4]_8$ (2.74−2.88 Å); these contacts are up to 0.43 Å shorter than $\sum R_{vdW}$ F···C (3.17 Å). Shorter distances in the gas-phase theoretical models as compared to the X-ray data are expected[39] and have been reported for other systems, for example, the fluoride selective cyclophane sandwich-type hosts reported by Mascal et al.[67]

The aforementioned findings point to the fact that the encapsulated $[BF_4]^-$ anion is critical for the stability of the metallacycle. The small cavity size of $[Fe_4(bptz)_4(CH_3CN)_8][BF_4]_8$, which favors short F···C anion−π contacts, and the tetrahedral geometry of $[BF_4]^-$ render it ideal for templation of a square by maximizing four F···C contacts per set of opposing tetrazine rings. The positioning of the $[BF_4]^-$ anion in the cavity, as well as the additivity of the anion−π contacts in $[Fe_4(bptz)_4(CH_3CN)_8][BF_4]_8$ (anion−π_4 system for each disorder position of the anion), which were established by the DFT studies, corroborate the importance of the anion−π interactions in the formation and stability of the tetranuclear $[\{Fe_4(bptz)_4(CH_3CN)_8\}\subset BF_4]^{7+}$ cation with the encapsulated anion.

Similarly, in $[\{Fe_5(bptz)_5(CH_3CN)_{10}\}\subset 2SbF_6][SbF_6]_8$, the close F···$C_{tetrazine}$ contacts of the encapsulated $[SbF_6]^-$ anions are also maximized with two tetrazine rings participating in two anion−π interactions and two tetrazine rings being involved in one such contact.[74] The two encapsulated $[SbF_6]^-$ anions fit tightly in the cavity of **2**, and each anion participates in three close F···C contacts with three F atoms oriented toward the C atoms of three tetrazine rings (Figure S9A) as well as in a longer F···C contact to an additional tetrazine ring. The average F···C distance is 2.91 Å, and the anion−ring distances are up to 0.36 Å shorter than $\sum R_{vdW}$ F···C (3.17 Å).[74] Each encapsulated anion is disordered between two positions in a way that allows it to engage in several short F···C anion−π contacts with the electropositive C atoms of the bptz tetrazine rings. Evidently, the geometry of the octahedral $[SbF_6]^-$ anion is better suited than a tetrahedral one to engage in anion−π contacts with the pentagonal π-acidic cavity. The positioning of the $[SbF_6]^-$ anion can be better appreciated in the reported structure of the metallacycle $[\{Fe_5(bmtz)_5(CH_3CN)_{10}\}\subset SbF_6][SbF_6]_9$ [bmtz = 3,6-bis(2-pyrimidyl)-1,2,4,5-tetrazine];[74] in this case, two F atoms of the well-ordered octahedral $[SbF_6]^-$ ion are lying over the electropositive C atoms of one tetrazine ring (exhibiting two short F···C contacts); each of the remaining four rings establishes one short F···C contact with the encapsulated anion, thereby having all five edges of the polygon engaged in anion−π interactions. Two F···$C_{tetrazine}$ close contacts with each of the two tetrazine rings were also located in the geometry-optimized binary adducts $C_2N_4R_2\cdots[PF_6]^-\cdots C_2N_4R_2$ (R = F, CN) wherein the substituted tetrazine moieties are eclipsed, thereby maximizing the F···$C_{tetrazine}$ contacts between the $[PF_6]^-$ anion and both tetrazine rings (two per ring; Figures 13B and S23B). In the crystal structures of the pentagonal metallacycles, however, the opposing tetrazine moieties (and thus the bptz ligands) are rotated by 60° with respect to each other because of the structural constraints imposed by the bptz chelation to the metal centers. Despite this situation and the fact that the $[SbF_6]^-$ anion in the pentagons is larger than $[PF_6]^-$, the computationally derived $R_{F\cdots C(tetrazine)}$ distances (∼2.7−2.8 Å) in the geometry-optimized binary adducts $C_2N_4R_2\cdots[PF_6]^-\cdots C_2N_4R_2$ are only by ∼0.1 Å shorter than the crystallographically determined F···$C_{tetrazine}$ distances for $[\{Fe_5(bptz)_5(CH_3CN)_{10}\}\subset 2SbF_6][SbF_6]_8$ (∼2.8−2.9 Å); this is an expected difference as indicated in the previous discussion for the $[BF_4]^-$ anions in the square cavity.[39,67a] As in the case of $[Fe_4(bptz)_4(CH_3CN)_8][BF_4]_8$, the small cavity size for the Fe(II) pentagons allows for short anion−π contacts. Moreover, the optimal positioning of the octahedral $[SbF_6]^-$ anion(s) leads to multiple short F···C contacts with the π-acidic tetrazine edges, and the additivity of the established anion−π contacts (anion−π_8 and −π_6 for $[\{Fe_5(bptz)_5(CH_3CN)_{10}\}\subset 2SbF_6][SbF_6]_8$ and $[\{Fe_5(bmtz)_5(CH_3CN)_{10}\}\subset SbF_6][SbF_6]_9$, respectively) confirms the importance of the anion identity as well as of the anion−π interactions in stabilizing the pentagonal metallacycles, despite their inherent angle strain and counterintuitive nuclearity.

Probing Anion−π Contacts in the Metallacycles by MAS ^{19}F NMR Spectroscopy. To our knowledge, until the present studies, X-ray crystallography was the sole method to detect anion−π interactions in the solid state, and the application of MAS NMR spectroscopy to study them is unprecedented. In general, the use of MAS NMR spectroscopy has experienced limited success in providing information at the molecular level for supramolecular systems with noncovalent interactions, because of technical difficulties and the fact that the interactions are highly anisotropic in the solid state, which in many cases leads to broad featureless spectra.[115] These hurdles notwithstanding, we set out to acquire MAS ^{19}F NMR spectra for the structurally characterized Fe(II) metallacycles $[Fe_4(bptz)_4(CH_3CN)_8][BF_4]_8$ and $[Fe_5(bptz)_5(CH_3CN)_{10}][SbF_6]_{10}$ with the goal of probing the chemical environment of the encapsulated anions. The MAS ^{19}F NMR data for the diamagnetic molecular square $[Zn_4(bptz)_4(CH_3CN)_8][BF_4]_8$ were also collected, primarily to test the possible paramagnetic effects of the Fe(II) atoms on the MAS spectra, which were, however, ruled out.

The room-temperature ^{19}F MAS NMR spectrum of a solid sample of $[\{Fe_4(bptz)_4(CH_3CN)_8\}\subset BF_4][BF_4]_7$ exhibits a broad nonsymmetrical resonance, which is resolved into three overlapping resonances with chemical shifts $\delta \approx 13.1$, 11.4, and 9.7 ppm (relative intensities 1:3:4; Figure S16b). These MAS ^{19}F NMR data are in good agreement with the single-crystal X-ray structural findings for $[\{Fe_4(bptz)_4(CH_3CN)_8\}\subset BF_4][BF_4]_7$, which revealed one encapsulated, four peripheral, and three interstitial $[BF_4]^-$ anions (Figures S6 and S7). It is reasonable to assign the most downfield ^{19}F NMR resonance at $\delta \approx 13.1$ ppm (with intensity 1) to the encapsulated $[BF_4]^-$ ion in the cavity of the metallacycle (Figures 1−3), the upfield ^{19}F NMR resonance at $\delta \approx 9.7$ ppm to the four $[BF_4]^-$ anions that are packed close to the outer edges of the cavity (Figure S6), and the third resonance at $\delta \approx 11.4$ ppm to the remaining three interstitial $[BF_4]^-$ ions (Figure S7). As detailed in the X-ray crystallography section, the encapsulated $[BF_4]^-$ anions have their F atoms in close F···C contacts with the C atoms of the opposing tetrazine rings at an average distance of F···C ≈ 2.84 Å (Figure 3); the presence and strength of these noncovalent interactions with the encapsulated $[BF_4]^-$ anion (anion−π_4 system for each anion) are reflected by the ^{19}F NMR downfield resonance at $\delta \approx 13.1$ ppm (with intensity 1), which is shifted by $\Delta\delta(^{19}F) \approx 3.4$ ppm from the ^{19}F NMR resonance of the four $[BF_4]^-$ anions, participating in short F···C contacts with both the tetrazine and pyridyl rings at the Fe(II) square peripheral edges.

dx.doi.org/10.1021/ja3082473 | J. Am. Chem. Soc. 2013, 135, 3039−3055

Similarly, the appearance of three different ^{19}F MAS NMR resonances for the $[BF_4]^-$ ions in the spectrum of $[\{Zn_4(bptz)_4(CH_3CN)_8\}\subset BF_4][BF_4]_7$ is in accord with the X-ray crystal structure.[73] From the inversion–recovery ^{19}F NMR spectrum, it is concluded that three resonances at $\delta \approx$ 12.4, 11.1, and 9.5 ppm are present in the partially relaxed MAS spectrum for $[\{Zn_4(bptz)_4(CH_3CN)_8\}\subset BF_4][BF_4]_7$ (Figure S15c). It is reasonable to assign the lowest field ^{19}F NMR resonance at $\delta \approx$ 12.4 ppm, with the slightly smaller T_1, to the encapsulated $[BF_4]^-$ ions that participate in the close F···C anion–π contacts with the tetrazine rings.[73] The other two ^{19}F NMR resonances at $\delta \approx$ 11.1 and 9.5 ppm are assigned to the $[BF_4]^-$ anions that are located near the outer edges of the square and to the remaining interstitial $[BF_4]^-$ ions as in the case of $[\{Fe_4(bptz)_4(CH_3CN)_8\}\subset BF_4][BF_4]_7$.

The three resonances with chemical shifts $\delta \approx$ 43.3, 40.0, and 39.4 ppm, that can be obtained from the analysis of the ^{19}F MAS NMR spectrum for $[\{Fe_5(bptz)_5(CH_3CN)_{10}\}\subset 2SbF_6][SbF_6]_8$ (Figures S17c and S18), and integrate in the ratio ~1:1.6:2.5 (approximately 2:3:5), indicate the presence of three types of inequivalent $[SbF_6]^-$ ions in this ratio, in agreement with the X-ray data for **2**. In particular, the downfield ^{19}F MAS NMR resonance at $\delta \approx$ 43.3 ppm and integration intensity of 2 can be assigned to the two encapsulated $[SbF_6]^-$ anions nestled inside the cavity of the polygon (Figures 4 and S9A) and in close F···C π contacts with the π-acidic tetrazine edges (anion–π_4 for each encapsulated anion). The upfield resonance at $\delta \approx$ 39.4 ppm, with relative intensity 5, is shifted by $\Delta\delta(^{19}F) \approx$ 3.9 ppm with respect to the ^{19}F NMR resonance for the two encapsulated anions and is attributed to the five $[SbF_6]^-$ anions that participate in short F···C contacts with the tetrazine rings only at the outer periphery of the Fe(II) pentagons (contacts marked with colored dotted lines in Figure S9B). Finally, the third ^{19}F MAS NMR resonance at $\delta \approx$ 40.0 ppm, with relative intensity 3, is assigned to the three $[SbF_6]^-$ anions that participate in short F···C contacts at the outer periphery of the Fe(II) pentagons with both the tetrazine and outer pyridyl rings (Figure S9B).

In summary, by applying ^{19}F MAS NMR spectroscopy, we garnered direct evidence of the different types of anions in the solid state despite only subtle differences in their environments; in particular, the ^{19}F MAS NMR resonances for the encapsulated anions in the cationic entities of **1** and **2** are shifted downfield by $\Delta\delta(^{19}F) \approx$ 3.5–4.0 ppm as compared to the peripheral anions. These shifts $\Delta\delta(^{19}F)$ for the encapsulated anions, engaged in anion–π contacts with the cavities, compare well with the corresponding shifts $\Delta\delta(^{1}H) \approx$ 3–5 ppm observed for various intermolecular noncovalent interactions in the solid state, such as hydrogen-bonding, π–π, and host–guest interactions.[115] Thus, the use of ^{19}F MAS NMR spectroscopy to discriminate different types of anions, exhibiting subtle differences due to short F···C anion–π contacts, proved to be highly useful in tandem with X-ray crystallography.

Monitoring the Interconversions of the Fe(II) Metallacycles in Solution by ^{1}H NMR Spectroscopy. X-ray crystallographic studies revealed that small anions[109] such as $[BF_4]^-$ and $[ClO_4]^-$ yield Fe(II) molecular squares, whereas the larger $[SbF_6]^-$ favors formation of the pentagon. The mass spectrometric data clearly point to the existence of $[Fe_4]^{8+}$ moieties in solution in the presence of the tetrahedral $[BF_4]^-$ and $[ClO_4]^-$ anions (Figures S1 and S5) and $[Fe_5]^{10+}$ units with the octahedral anions $[SbF_6]^-$, $[PF_6]^-$, and $[AsF_6]^-$ (Figures S2–S4). No evidence for higher-nuclearity species or the coexistence of squares and pentagons in the presence of each anion was found. Furthermore, the competing influence of the anions in stabilizing Fe(II) metallacycles of different nuclearities as well as the interconversions between square and pentagon metallacycles, in the presence of the appropriate anions, was successfully probed in solution by ^{1}H NMR spectroscopy. To our knowledge, this is the first time that such studies for anion-templated metallacycles have been monitored by applying NMR methods.

The exceptional stability of $[Fe_5(bptz)_5(CH_3CN)_{10}][SbF_6]_{10}$ is evidenced by the absence of ^{1}H NMR resonances for the square $[Fe_4(bptz)_4(CH_3CN)_8][BF_4]_8$ despite overnight stirring of the pentagon sample with a 15-fold excess of $[n\text{-}Bu_4N][BF_4]$. Only after refluxing the metallapentacycle for 4 h with a 25-fold excess of $[n\text{-}Bu_4N][BF_4]$ is complete conversion to the square achieved (Figure 7). Further evidence for the remarkable stability of the pentagon unit is the fact that a ~50:50% mixture of $[Fe_4(bptz)_4(CH_3CN)_8][BF_4]_8/[Fe_5(bptz)_5(CH_3CN)_{10}][SbF_6]_{10}$ forms when $[Fe_4(bptz)_4(CH_3CN)_8][BF_4]_8$ is refluxed with a 16-fold excess of $[n\text{-}Bu_4N][SbF_6]$ for 2 or 4 days, as determined by ^{1}H NMR spectroscopy (Figure 8b,c). These results for the Fe(II) metallacycles can be contrasted with the corresponding interconversion ESI-MS studies of the Ni(II) congeners: complete conversion of the Ni(II) pentagon to the square analog is easily achieved by mere stirring of a $[Ni_5(bptz)_5(CH_3CN)_{10}][SbF_6]_{10}$ solution for several minutes in the presence of excess $[BF_4]^-$ or $[ClO_4]^-$ anions. Moreover, only small quantities of the Ni(II) pentagon are detected by ESI-MS after refluxing a $[Ni_4(bptz)_4(CH_3CN)_8][BF_4]_8$ solution with a 50-fold excess of $[SbF_6]^-$ anions for 2 days. Even after 5 days of reflux, the product distribution favors the Ni(II) square as evidenced by ESI-MS.[73]

An even more notable finding is that the Fe(II) pentagon templated by $[AsF_6]^-$ is more stable than that templated by $[SbF_6]^-$, as mere overnight stirring of $[Fe_4(bptz)_4(CH_3CN)_8][BF_4]_8$ with a 15-fold excess of $[AsF_6]^-$ anions at +55 °C results in a ~44:56% ratio of $[Fe_4(bptz)_4(CH_3CN)_8][BF_4]_8/[Fe_5(bptz)_5(CH_3CN)_{10}][AsF_6]_{10}$ in solution (Figure 9). Additionally, although a Ni(II) metallacycle templated by $[PF_6]^-$ anions was not detected in our earlier studies,[73] in the case of Fe(II), the NMR, CV, and ESI-FT-ICR-MS data (Figures 6c, S21, and S3, respectively) support the formation of the pentagon $[Fe_5(bptz)_5(CH_3CN)_{10}][PF_6]_{10}$ despite its relatively low stability. The small quantities of partially open metallacycle apparent in the ^{1}H NMR spectrum (Figure 6c), the quasi-reversible oxidation event at higher potential in the electrochemical data, and the thermal sensitivity of $[Fe_5(bptz)_5(CH_3CN)_{10}][PF_6]_{10}$, which prevented any interconversion studies from being conducted, attest to its lower stability as compared to the pentagonal metallacycles with other templating anions.

The aforementioned data gleaned from the ^{1}H NMR studies lead to the following order of stability for the Fe(II) pentagons: $[Fe_5(bptz)_5(CH_3CN)_{10}][PF_6]_{10} \ll [Fe_5(bptz)_5(CH_3CN)_{10}][SbF_6]_{10} < [Fe_5(bptz)_5(CH_3CN)_{10}][AsF_6]_{10}$. From this ordering, taking into consideration the relative anion sizes {i.e., $[PF_6]^-$ (54 Å^3) < $[AsF_6]^-$ (63 Å^3) < $[SbF_6]^-$ (71 Å^3)},[109] it is concluded that the $[AsF_6]^-$ ions provide the optimal anion–π contacts with the Fe(II) pentagonal cavity, followed by $[SbF_6]^-$. The $[PF_6]^-$ anion is apparently too small to template a very stable Fe(II) pentagon (yet too large to template an Fe(II) square). It is noteworthy, however, that the templation

dx.doi.org/10.1021/ja3082473 | J. Am. Chem. Soc. 2013, 135, 3039–3055

of the metallapentacycles is not merely a matter of anion size but rather a synergistic combination of shape, size, and symmetry of the encapsulated anion and its potential to establish short anion−π contacts. This conclusion is supported by the fact that, although the $[CF_3SO_3]^-$ anion (68 Å^3)[90] is comparable in size with $[AsF_6]^-$ (63 Å^3) and $[SbF_6]^-$ (71 Å^3), which are known to lead to pentagons,[110] $[CF_3SO_3]^-$ does not support polygon templation, as revealed by the NMR spectroscopic data (Figure 10a). Formation of the polygons $[Fe_5(bptz)_5(CH_3CN)_{10}][AsF_6]_{10}$, $[Fe_5(bptz)_5(CH_3CN)_{10}][SbF_6]_{10}$, and $[Fe_4(bptz)_4(CH_3CN)_8][BF_4]_8$ takes place, however, upon addition of the suitable templating anions, namely, $[AsF_6]^-$, $[SbF_6]^-$, and $[BF_4]^-$, respectively (Figures 10b−d, respectively). These data thus provide unequivocal confirmation of anion-based templation for the aforementioned metallacycles.

Additionally, the reduction of the cavity size due to the M−N (M = Zn, Ni, Fe) distances contracting in the order Zn(II) > Ni(II) ≫ Fe(II) also agrees well with the fact that the $[PF_6]^-$ anion does not template a Ni(II) metallacycle[73] and that a Zn(II) pentagon with $[SbF_6]^-$ anions does not form owing to the fact that the Ni(II) and Zn(II) cavities would be too large to be templated by the corresponding anions. It is also noted that the ligand lability of Zn(II) and Ni(II) ions as compared to LS Fe(II) ions is higher, which is expected to contribute to the reduced relative stability of $[Ni_5(bptz)_5(CH_3CN)_{10}][SbF_6]_{10}$ as compared to $[Fe_5(bptz)_5(CH_3CN)_{10}][SbF_6]_{10}$ (vide supra) and the absence of a Zn(II) pentagon. The foregoing comparative correlations provide compelling evidence for the importance of establishing an optimum anion/cavity close orientation, allowing for short anion−π contacts, and reinforce our contention that the latter play a pivotal role in stabilizing the metallacycles.

^{19}F NMR Spectroscopy of the Fe(II) Metallacycles in Solution. The considerable broadening of the ^{19}F NMR resonance for $[Fe_4(bptz)_4(CH_3CN)_8][BF_4]_8$ at $\delta \approx -150$ ppm with increasing temperature, in the range between +20 and −40 °C (Figure S12), indicates rapid exchange of the encapsulated $[BF_4]^-$ anions with the free species on the time scale of the NMR experiment,[88,96] in accord with the smallest square Fe(II) cavity among the polygons and its high occupancy by the guest.[110] The fast exchange of the $[BF_4]^-$ anion is presumably facilitated by its off-center positioning in the cavity and the anion being rather closer to the open face of the polygon as indicated by the X-ray crystal structure (Figure 2). Additionally, upon lowering the temperature, the polygons $[Fe_5(bptz)_5(CH_3CN)_{10}][PF_6]_{10}$ (Figure S13) and $[Zn_4(bptz)_4(CH_3CN)_8][BF_4]_8$ exhibit broadening of the ^{19}F NMR resonances, and each metallacycle exhibits a second distinct ^{19}F NMR resonance of lower intensity, which corroborates the presence of encapsulated anions. The calculated anion-exchange rates[98,116] are $k_{exc(BF_4)} = 140(14)$ s^{-1} (at 238 K) and $k_{exc(PF_6)} = 166(16)$ s^{-1} (at 233 K), yielding activation energies of encapsulation $\Delta G^{\ddagger}_{238K(BF_4)} = 48(4)$ kJ/mol and $\Delta G^{\ddagger}_{233\ K(PF_6)} = 46(4)$ kJ/mol for $[Zn_4(bptz)_4(CH_3CN)_8][BF_4]_8$ and $[Fe_5(bptz)_5(CH_3CN)_{10}][PF_6]_{10}$, respectively. The aforementioned low activation energy values confirm that the exchange involves diffusion of the anions through the open faces of the intact metallacyclic cages without cleavage of the M−N coordination bonds, which would require considerably higher activation energies. The determined low activation energies of encapsulation for the anions ($\Delta G^{\ddagger} \approx 50$ kJ/mol) are in the expected energy range for anion−π interactions (~20−70 kJ/mol[33c]), which corroborates anion encapsulation in the metallacycle cavities by noncovalent contacts.

CONCLUSIONS

The results of the studies reported herein provide unambiguous evidence that anion−π interactions are the main driving force in the templation process leading to the formation of Fe(II) metallacycles with π-acidic cavities spanned by the divergent chelating ligand bptz. Comprehensive studies conducted both in the solid state and in solution support the contention that the templating anions play a decisive role in the formation and identity of the polygons. It was demonstrated by X-ray crystallography, ^{1}H and ^{19}F NMR spectroscopies in solution, ^{19}F MAS NMR spectroscopy, and CV and mass spectrometry studies that the anions $[X]^- = [BF_4]^-$ and $[ClO_4]^-$ template the molecular squares $[Fe_4(bptz)_4(CH_3CN)_8][X]_8$, whereas the larger anions $[Y]^- = [SbF_6]^-$, $[AsF_6]^-$, and $[PF_6]^-$ induce formation of the molecular pentagons $[Fe_5(bptz)_5(CH_3CN)_{10}][Y]_{10}$ in high yields.

The X-ray crystal structures of $[\{Fe_4(bptz)_4(CH_3CN)_8\}\subset BF_4][BF_4]_7$ and $[\{Fe_5(bptz)_5(CH_3CN)_{10}\}\subset 2SbF_6][SbF_6]_8$ revealed that the corresponding encapsulated $[BF_4]^-$ and $[SbF_6]^-$ anions are tightly packed in the cavities of the metallacycles and that their F atoms are within van der Waals contact with the tetrazine C atoms of the bptz entities (by up to ~0.4 Å shorter than $\sum R_{vdW}$ F···C = 3.17 Å). The encapsulated anions occupy the π-acidic cavities at optimal locations, which results in the maximum number and strength of close directional F···C contacts with all the central bptz rings. The F atoms of the encapsulated anions are directly located over the more π-acidic tetrazine C atoms, establishing additive anion−π_6 or −π_4 contacts with the metallacycle edges. The F···C distances and the positioning of the anions with respect to the opposing tetrazine rings at the polygon edges derived from the X-ray data are in excellent agreement with the DFT calculations performed on the optimized binary adducts $C_2N_4R_2\cdots[X]^-\cdots C_2N_4R_2$ (R = F, CN; $[X]^- = [BF_4]^-$, $[PF_6]^-$). Additionally, the close contacts of the anions to the π-acidic rings in the solid state were probed by ^{19}F MAS NMR spectroscopy, which, to our knowledge, is the first example of such studies. The ^{19}F MAS NMR resonances for the encapsulated anions, involved in the anion−π contacts, are shifted downfield by $\Delta\delta(^{19}F) \approx 3.5$−4.0 ppm as compared to the peripheral anions of the polygons; these shifts correlate well with the fact that the anions are engaged in noncovalent interactions in the solid state.

Evidence for anion-based templation in solution and the instrumental role of the templating anions in favoring and stabilizing Fe(II) metallacycles of specific nuclearities was obtained by the application of NMR spectroscopy for the first time. Notably, random Fe(II)/bptz oligomers are formed in the presence of non-templating anions (e.g., $[CF_3SO_3]^-$), and self-assembly of the respective closed polygons is *not* activated unless the appropriate templating anions (e.g., $[BF_4]^-$, $[AsF_6]^-$, $[SbF_6]^-$) are added to the solution. We thus conclude with confidence that the appropriate anions act as templates rather than merely diffusing into preformed cages[90,95,111,116] and that they constitute an essential directing element in the polygon self-assembly.

Additionally, interconversion solution studies between the square and pentagonal Fe(II) metallacycles in the presence of excess amounts of the appropriate anions unearthed the fact that the pentagonal structural units are remarkably stable. The

dx.doi.org/10.1021/ja3082473 | J. Am. Chem. Soc. 2013, 135, 3039−3055

relative order of stability was found to be $[Fe_5(bptz)_5(CH_3CN)_{10}][PF_6]_{10} \ll [Fe_5(bptz)_5(CH_3CN)_{10}][SbF_6]_{10} < [Fe_5(bptz)_5(CH_3CN)_{10}][AsF_6]_{10}$, which is in accord with the anion sizes ($[PF_6]^- < [AsF_6]^- < [SbF_6]^-$) and optimal cavity size/anion–π contacts. Apart from the ^{1}H NMR evidence, cyclic voltammetric and mass spectrometric studies firmly established that the Fe(II) metallacycles remain as discrete, stable, and intact entities in solution and form polygons of only a single nuclearity in the presence of each anion. Moreover, the electrochemical studies indicate that the π-acidity of the bound bptz ligands is reduced, despite the electron donation to the coordinated metal atoms, which is attributed to the anion–π contacts with the encapsulated anions. The combined results of all the aforementioned experiments provide strong corroboration for our contention that the Fe(II) metallacycles are very stable in solution and, in particular, that the pentagons are very robust, which is remarkable, considering their inherent angle strain as compared to the more commonly encountered square motif. Finally, the low activation energies of encapsulation for the anions ($\Delta G^{\ddagger} \approx 50$ kJ/mol), which are in the expected energy range for anion–π interactions (~20–70 kJ/mol), confirm that the anions in the π-acidic metallacycle cavities studied herein engage in anion–π contacts that drive the formation of a particular polygon product.

■ ASSOCIATED CONTENT

Supporting Information

Figures S1–S5: ESI-FT-ICR-MS spectra for polygons. Figures S6 and S9: outer-sphere ion F···C contacts with bptz in **1** and **2**. Figures S7 and S8: Packing diagrams for **1** and **2**. Figures S10 and S11: ^{1}H NMR spectra of $[Zn(CH_3CN)_4][SbF_6]_2$ and bptz before and after addition of excess $[n\text{-}Bu_4N][BF_4]$. Figures S12 and S13: VT ^{19}F NMR spectra of $[Fe_4(bptz)_4(CH_3CN)_8][BF_4]_8$ and $[Fe_5(bptz)_5(CH_3CN)_{10}][PF_6]_{10}$. Figure S14: ^{19}F NMR spectrum of $[Ag_2(bptz)_3][SbF_6]_2$. Figures S15–S18: ^{19}F MAS NMR spectra and comments. Figures S19–S21: Electrochemical data for Fe(II) polygons. Figures S22 and S23: DFT data of geometry-optimized complexes $C_2N_4F_2\cdots[X]^-$ and $C_2N_4F_2\cdots[X]^-\cdots C_2N_4R_2$, $[X]^- = [BF_4]^-$ or $[PF_6]^-$. Figure S24: ESP maps of $C_2N_4R_2$ (R = F, CN). Tables S1–S3: Crystal data, structural refinement parameters, and bond distances and angles for **1** and **2**. Full citation for Gaussian and other references. This material is available free of charge via the Internet at http://pubs.acs.org. Compounds deposited with the Cambridge Crystallographic Data Centre (CCDC): **1**, 879374; **2**, 844757.

■ AUTHOR INFORMATION

Corresponding Author

chifotides@mail.chem.tamu.edu; dunbar@mail.chem.tamu.edu

Notes

The authors declare no competing financial interest.

■ ACKNOWLEDGMENTS

K.R.D. gratefully acknowledges the Robert A. Welch Foundation for support of this project (Grant A-1449). We sincerely acknowledge Dr. Vladimir I. Bakhmutov for acquiring and analyzing the solid state NMR data as well as for helpful discussions. Professor Jonathan R. Nitschke and Dr. Borris Breiner are acknowledged for their instrumental help with the program Voidoo, and Dr. George A. Souliotis is acknowledged for running the Voidoo calculations on the polygons. Dr. Andrey Prosvirin is acknowledged for the magnetic measurements. We also thank Prof. Steven E. Wheeler, Dr. Brandi L. Schottel, and Dr. Lisa M. Pérez for helpful discussions in regard to the computational studies. The Supercomputing Facility and the Laboratory for Molecular Simulation at Texas A&M University are acknowledged for providing software and computer time. The use of the TAMU/LBMS-Applications Laboratory (Laboratory of Biological Mass Spectroscopy) is acknowledged.

■ REFERENCES

(1) (a) Chakrabarty, R.; Mukherjee, P. S.; Stang, P. J. *Chem. Rev.* **2011**, *111*, 6810–6918 and references therein. (b) Leininger, S.; Olenyuk, B.; Stang, P. J. *Chem. Rev.* **2000**, *100*, 853–908. (c) Stang, P. J.; Olenyuk, B. *Acc. Chem. Res.* **1997**, *30*, 502–518.

(2) (a) Pluth, M. D.; Raymond, K. N. *Chem. Soc. Rev.* **2007**, *36*, 161–171. (b) Davis, A. V.; Raymond, K. N. *Acc. Chem. Res.* **1999**, *32*, 975–982.

(3) (a) Fujita, M.; Tominaga, M.; Hori, A.; Therrien, B. *Acc. Chem. Res.* **2005**, *38*, 371–380. (b) Fujita, M.; Umemoto, K.; Yoshizawa, M.; Fujita, N.; Kusukawa, T.; Biradha, K. *Chem. Commun.* **2001**, 509–518.

(4) Holiday, B. J.; Mirkin, C. A. *Angew. Chem., Int. Ed.* **2001**, *40*, 2022–2043.

(5) (a) Lehn, J.-M. *Supramolecular Chemistry: Concepts and Perspectives*; VCH: Weinheim, Germany, 1995. (b) Lehn, J.-M. *Science* **2002**, *295*, 2400–2403. (c) Lehn, J.-M. *Chem. Soc. Rev.* **2007**, *36*, 151–160.

(6) Steed, J. W.; Atwood, J. L. *Supramolecular Chemistry*; Wiley: London, 2009.

(7) (a) Sun, Q.-F.; Sato, S.; Fujita, M. *Nat. Chem.* **2012**, *4*, 330–333. (b) Sun, Q.-F.; Iwasa, J.; Ogawa, D.; Ishido, Y.; Sato, S.; Ozeki, T.; Yoshihisa, S.; Yamaguchi, K.; Fujita, M. *Science* **2010**, *328*, 1144–1147. (c) Takeda, N.; Umemoto, K.; Yamaguchi, K.; Fujita, M. *Nature* **1999**, *398*, 794–796.

(8) (a) Kuehl, C. J.; Kryshenko, Y. K.; Radhakrishnan, U.; Seidel, S. R.; Huang, S. D.; Stang, P. J. *Proc. Natl. Acad. Sci. U.S.A.* **2002**, *99*, 4932–4936. (b) Olenyuk, B.; Whiteford, J. A.; Fechtenkotter, A.; Stang, P. J. *Nature* **1999**, *398*, 796–799.

(9) (a) Cotton, F. A.; Lin, C.; Murillo, C. A. *Acc. Chem. Res.* **2001**, *34*, 759–771. (b) Cotton, F. A.; Lin, C.; Murillo, C. A. *Proc. Natl. Acad. Sci. U.S.A.* **2002**, *99*, 4810–4813.

(10) (a) Ruben, M.; Lehn, J.-M.; Müller, P. *Chem. Soc. Rev.* **2006**, *35*, 1056–1067. (b) Ruben, M.; Rojo, J.; Romero-Salguero, F. J.; Uppadine, L. H.; Lehn, J.-M. *Angew. Chem., Int. Ed.* **2004**, *43*, 3644–3662. (c) Ruben, M.; Breuning, E.; Lehn, J.-M.; Ksenofontov, V.; Renz, F.; Gütlich, P.; Vaughan, G. B. M. *Chem.—Eur. J.* **2003**, *9*, 4422–4429. (d) Breuning, E.; Ruben, M.; Lehn, J.-M.; Renz, F.; Garcia, Y.; Ksenofontov, V.; Gütlich, P.; Wegelius, E.; Rissanen, K. *Angew. Chem., Int. Ed.* **2000**, *39*, 2504–2507.

(11) Wei, R.-J.; Huo, Q.; Tao, J.; Huang, R.-B.; Zheng, L.-S. *Angew. Chem., Int. Ed.* **2011**, *50*, 8940–8943.

(12) Steed, J. W. *Chem. Soc. Rev.* **2009**, *38*, 506–519.

(13) (a) Nguyen, S.-B. T.; Gin, D. L.; Hupp, J. T.; Zhang, X. *Proc. Natl. Acad. Sci. U.S.A.* **2001**, *98*, 11849–11850. (b) Slone, R. V.; Benkstein, K. D.; Bélanger, S.; Hupp, J. T.; Guzei, I. A.; Rheingold, A. L. *Coord. Chem. Rev.* **1998**, *171*, 221–243.

(14) Nihei, M.; Ui, M.; Yokota, M.; Han, L.; Maeda, A.; Kishida, H.; Okamoto, H.; Oshio, H. *Angew. Chem.* **2005**, *117*, 6642–6645.

(15) (a) Pluth, M. D.; Bergman, R. G.; Raymond, K. N. *Acc. Chem. Res.* **2009**, *42*, 1650–1659. (b) Davis, A. V.; Raymond, K. N. *J. Am. Chem. Soc.* **2005**, *127*, 7912–7919.

(16) (a) Meng, W.; Breiner, B.; Rissanen, K.; Thoburn, J. D.; Clegg, J. K.; Nitschke, J. R. *Angew. Chem., Int. Ed.* **2011**, *50*, 3479–3483. (b) Breiner, B.; Clegg, J. K.; Nitschke, J. R. *Chem. Sci.* **2011**, *2*, 51–56. (c) Bilbeisi, R. A.; Clegg, J. K.; Elgrishi, N.; de Hatten, X.; Devillard, M.; Breiner, B; Mal, P.; Nitschke, J. R. *J. Am. Chem. Soc.* **2012**, *134*, 5110–5119. (d) Meng, W.; Clegg, J. K.; Nitschke, J. R. *Angew. Chem., Int. Ed.* **2012**, *51*, 1881–1884.

(17) Rebek, J., Jr. *Acc. Chem. Res.* **2009**, *42*, 1660−1668.
(18) Zhao, L.; Ghosh, K.; Zheng, Y.; Lyndon, M. M.; Williams, T. I.; Stang, P. J. *Inorg. Chem.* **2009**, *48*, 5590−5592.
(19) (a) Hwang, S.-H.; Wang, P.; Moorefield, C. N.; Godínez, L. A.; Manriquez, J.; Bustos, E.; Newkome, G. R. *Chem. Commun.* **2005**, 4672−4674. (b) Li, X.; Chan, Y.-T.; Casiano-Maldonado, M.; Yu, J.; Carri, G. A.; Newkome, G. R.; Wesdemiotis, C. *Anal. Chem.* **2011**, *83*, 6667−6674.
(20) (a) Hasenknopf, B.; Lehn, J.-M.; Kneisel, O.; Baum, G.; Fenske, D. *Angew. Chem., Int. Ed.* **1996**, *35*, 1838−1840. (b) Hasenknopf, B.; Lehn, J.-M.; Boumediene, N.; Dupont-Gervais, A.; Dorsselaer, A. V.; Kneisel, B.; Fenske, D. *J. Am. Chem. Soc.* **1997**, *119*, 10956−10962.
(21) Ayme1, J.-F.; Beves, J. E.; Leigh, D. A.; McBurney, R. T.; Rissanen, K.; Schultz, D. *Nat. Chem.* **2012**, *4*, 15−20.
(22) Riddell, I. A.; Smulders, M. M. J.; Clegg, J. K.; Hristova, Y. R.; Breiner, B.; Thoburn, J. D.; Nitschke, J. R. *Nat. Chem.* **2012**, *4*, 751−756.
(23) Furlan, R. L. E.; Otto, S.; Sanders, J. K. M. *Proc. Natl. Acad. Sci. U.S.A.* **2002**, *99*, 4801−4804.
(24) (a) Vilar, R. *Angew. Chem., Int. Ed.* **2003**, *42*, 1460−1477. (b) Vilar, R. *Coord. Chem. Rev.* **2006**, *250*, 3161−3189. (c) Vilar, R. *Struct. Bonding (Berlin)* **2008**, *129*, 175−206. (d) Vilar, R. *Eur. J. Inorg. Chem.* **2008**, *3*, 357−367.
(25) Paul, R. L.; Bell, Z. R.; Jeffery, J. C.; McCleverty, J. A.; Ward, M. D. *Proc. Natl. Acad. Sci. U.S.A.* **2002**, *99*, 4883−4888.
(26) Hiraoka, S.; Fujita, M. *J. Am. Chem. Soc.* **1999**, *121*, 10239−10240.
(27) Amouri, H.; Desmarets, C.; Bettoschi, A.; Rager, M. N.; Boubekeur, K.; Rabu, P.; Drillon, M. *Chem.—Eur. J.* **2007**, *13*, 5401−5407.
(28) Amouri, H.; Mimassi, L.; Rager, M. N.; Mann, B. E.; Guyard-Duhayon, C.; Raehm, L. *Angew. Chem., Int. Ed.* **2005**, *44*, 4543−4546.
(29) (a) Gale, P. A. *Coord. Chem. Rev.* **2003**, *240*, 1−2. (b) Wenzel, M.; Hiscock, J. R.; Gale, P. A. *Chem. Soc. Rev.* **2012**, *41*, 480−520.
(30) (a) Atwood, J. L.; Steed, J. W. Structural and Topological Aspects of Anion Coordination in *Supramolecular Chemistry of Anions*; Bianchi, A., Bowman-James, K., García-España, E., Eds.; John Wiley−VCH: New York, 1997; pp 147−215. (b) Arranz-Mascarós, P.; Bazzicalupi, C.; Bianchi, A.; Giorgi, C.; Godino-Salido, M.-L.; Gutiérrez-Valero, M.-D.; Lopez-Garzón, R.; Savastano, M. *J. Am. Chem. Soc.* **2013**, *135*, 102−105.
(31) Clegg, J. K.; Lindoy, L. F. Template Synthesis in *Anion Coordination Chemistry*; Bowman-James, K., Bianchi, A., García-España, E., Eds.; Wiley−VCH: Weinheim, Germany, 2012; Chapter 5, pp 289−320.
(32) (a) Schottel, B. L.; Chifotides, H. T.; Dunbar, K. R. *Chem. Soc. Rev.* **2008**, *37*, 68−83 and references therein. (b) Chifotides, H. T.; Dunbar, K. R. *Acc. Chem. Res.* **2013**, DOI: 10.1021/ar300251k.
(33) (a) Gamez, P.; Mooibroek, T. J.; Teat, S. J.; Reedijk, J. *Acc. Chem. Res.* **2007**, *40*, 435−444. (b) Mooibroek, T. J.; Black, C. A.; Gamez, P.; Reedijk, J. *Cryst. Growth Des.* **2008**, *8*, 1082−1093. (c) Frontera, A.; Gamez, P.; Mascal, M.; Mooibroek, T. J.; Reedijk, J. *Angew. Chem., Int. Ed.* **2011**, *50*, 9564−9583.
(34) (a) Robertazzi, A.; Krull, F.; Knapp, E.-W.; Gamez, P. *CrystEngComm* **2011**, *13*, 3293−3300. (b) Mooibroek, T. J.; Gamez, P. *CrystEngComm* **2012**, *14*, 3902−3906.
(35) (a) Quiñonero, D.; Frontera, A.; Costa, A.; Deyà, P. M. Anion−π Interactions in Molecular Recognition in *Anion Coordination Chemistry*; Bowman-James, K., Bianchi, A., García-España, E., Eds.; Wiley−VCH: Weinheim, Germany, 2012; Chapter 6, pp 321−361 and references therein. (b) Chakravarty, S.; Sheng, Z.-Z.; Iverson, B.; Moore, B. *FEBS Letters* **2012**, *586*, 4180−4185.
(36) Ballester, P. *Struct. Bonding (Berlin)* **2008**, *129*, 127−174.
(37) Alkorta, I.; Rozas, I.; Elguero, J. *J. Am. Chem. Soc.* **2002**, *124*, 8593−8598.
(38) Quiñonero, D.; Garau, C.; Rotger, C.; Frontera, A.; Ballester, P.; Costa, A.; Deyà, P. M. *Angew. Chem., Int. Ed.* **2002**, *41*, 3389−3392.
(39) Mascal, M.; Armstrong, A.; Bartberger, M. D. *J. Am. Chem. Soc.* **2002**, *124*, 6274−6276.
(40) Demeshko, S.; Dechert, S.; Meyer, F. *J. Am. Chem. Soc.* **2004**, *126*, 4508−4509.
(41) Casellas, H.; Massera, C.; Gamez, P.; Manotti Lanfredi, A. M.; Reedijk, J. *Eur. J. Inorg. Chem.* **2005**, 2902−2908.
(42) de Hoog, P.; Gamez, P; Mutikainen, I; Turpeinen, U.; Reedijk, J. *Angew. Chem., Int. Ed.* **2004**, *43*, 5815−5817.
(43) (a) Schottel, B. L.; Chifotides, H. T.; Shatruk, M.; Chouai, A.; Bacsa, J.; Pérez, L. M.; Dunbar, K. R. *J. Am. Chem. Soc.* **2006**, *128*, 5895−5912. (b) Schottel, B. L.; Bacsa, J.; Dunbar, K. R. *Chem. Commun.* **2005**, 46−47.
(44) Frontera, A.; Saczewski, F.; Gdaniec, M.; Dziemidowicz-Borys, E.; Kurland, A.; Deyà, P. M.; Quiñonero, D.; Garau, C. *Chem. Eur. J.* **2005**, *11*, 6560−6567.
(45) Fairchild, R. M.; Holman, K. T. *J. Am. Chem. Soc.* **2005**, *127*, 16364−14365.
(46) Staffilani, M.; Hancock, K. S. B.; Steed, J. W.; Holman, K. T.; Atwood, J. L.; Juneja, R. K.; Burkhalter, R. S. *J. Am. Chem. Soc.* **1997**, *119*, 6324−6335.
(47) Lenthall, J. T.; Steed, J. W. *Coord. Chem. Rev.* **2007**, *251*, 1747−1760.
(48) Götz, R. J.; Robertazzi, A.; Multikainen, I.; Turpeinen, U.; Gamez, P.; Reedijk, J. *Chem. Commun.* **2008**, 3384−3386.
(49) Barrios, L. A.; Aromí, G.; Frontera, A.; Quiñonero, D.; Deyà, P. M.; Gamez, P.; Roubeau, O.; Shotton, E. J.; Teat, S. J. *Inorg. Chem.* **2008**, *47*, 5873−5881.
(50) Estarellas, C.; Rotger, M. C.; Capó, M.; Quiñonero, D.; Frontera, A.; Costa, A.; Deyà, P. M. *Org. Lett.* **2009**, *11*, 1987−1990.
(51) (a) Gural'skiy, I. A.; Solntsev, P. V.; Krautscheid, H.; Domasevitch, K. V. *Chem. Commun.* **2006**, 4808−4810. (b) Gural'skiy, I. A.; Escudero, D.; Frontera, A.; Solntsev, P. V.; Rusanov, E. B.; Chernega, A. N.; Krautscheid, H.; Domasevitch, K. V. *Dalton Trans.* **2009**, 2856−2864.
(52) Moussa, J.; Gandon, V.; Rager, M. N.; Malacria, M.; Chamoreau, L.-M.; Amouri, H. *Eur. J. Inorg. Chem.* **2009**, 3703−3707.
(53) Hung, C.-Y.; Singh, A. S.; Chen, C.-W.; Wen, Y.-S.; Sun, S.-S. *Chem. Commun.* **2009**, 1511−1513.
(54) (a) Watt, M. M.; Collins, M. S.; Johnson, D. W. *Acc. Chem. Res.* **2012**, DOI: 10.1021/ar300100g. (b) Berryman, O. B.; Johnson, D. W. *Chem. Commun.* **2009**, 3143−3153. (c) Berryman, O. B.; Sather, A. C.; Hay, B. P.; Meisner, J. S.; Johnson, D. W. *J. Am. Chem. Soc.* **2008**, *130*, 10895−10897. (d) Berryman, O. B.; Hof, F.; Hynes, M. J.; Johnson, D. W. *Chem. Commun.* **2006**, 506−508.
(55) Rosokha, Y. S.; Lindeman, S. V.; Rosokha, S. V.; Kochi, J. K. *Angew. Chem., Int. Ed.* **2004**, *43*, 4650−4652.
(56) Lakshminarayanan, P. S.; Ravikumar, I.; Suresh, E.; Ghosh, P. *Inorg. Chem.* **2007**, *46*, 4769−4771.
(57) (a) Gil-Ramírez, G.; Escudero-Adán, E. C.; Benet-Buchholtz, J.; Ballester, P. *Angew. Chem., Int. Ed.* **2008**, *47*, 4114−4118. (b) Ballester, P. *Acc. Chem. Res.* **2012**, DOI: 10.1021/ar300080f.
(58) (a) Wang, D.-X.; Wang, M.-X. *J. Am. Chem. Soc.* **2013**, *135*, 892−897. (b) Wang, D.-X.; Wang, M.-X. *Chimia* **2011**, *65*, 939−943. (c) Wang, D.-X.; Zheng, Q.-Y.; Wang, Q.-Q.; Wang, M.-X. *Angew. Chem., Int. Ed.* **2008**, *47*, 7485−7488.
(59) (a) Frontera, A.; Quiñonero, D.; Deyà, P. M. *Wiley Interdiscip. Rev.: Comput. Mol. Sci.* **2011**, *1*, 440−459 and references therein. (b) Garau, C.; Frontera, A.; Quiñonero, D.; Ballester, P.; Costa, A.; Deyà, P. M. *Recent Res. Dev. Chem. Phys.* **2004**, *5*, 227−255.
(60) Estarellas, C.; Bauzà, A.; Frontera, A.; Quiñonero, D.; Deyà, P. M. *Phys. Chem. Chem. Phys.* **2011**, *13*, 5696−5702.
(61) Berryman, O. B.; Bryantsev, V. S.; Stay, D. P.; Johnson, D. W.; Hay, B. P. *J. Am. Chem. Soc.* **2007**, *129*, 48−58.
(62) (a) Wheeler, S. E.; Houk, K. N. *J. Phys. Chem.* **2010**, *114*, 8658−8664. (b) Wheeler, S. E. *Acc. Chem. Res.* **2012**, DOI: 10.1021/ar300109n.
(63) Chifotides, H. T.; Schottel, B. L.; Dunbar, K. R. *Angew. Chem., Int. Ed.* **2010**, *49*, 7202−7207.
(64) (a) Guha, S.; Goodson, F. S.; Corson, L. J.; Saha, S. *J. Am. Chem. Soc.* **2012**, *134*, 13679−13691. (b) Guha, S.; Goodson, F. S.; Roy, S.; Corson, L. J.; Gravenmier, C. A.; Saha, S. *J. Am. Chem. Soc.* **2011**, *113*,

15256−15259. (c) Guha, S.; Saha, S. *J. Am. Chem. Soc.* **2010**, *132*, 17674−17677.
(65) Jentzsch, A. V.; Emery, D.; Mareda, J.; Metrangolo, P.; Resnati, G.; Matile, S. *Angew. Chem., Int. Ed.* **2011**, *50*, 11675−11678.
(66) Chudzinski, M. G.; McClary, C. A.; Taylor, M. S. *J. Am. Chem. Soc.* **2011**, *133*, 10559−10567.
(67) (a) Mascal, M.; Yakovlev, I.; Nikitin, E. B.; Fettinger, J. C. *Angew. Chem., Int. Ed.* **2007**, *46*, 8782−8784. (b) Mascal, M. *Angew. Chem., Int. Ed.* **2006**, *45*, 2890−2893.
(68) Perraud, O.; Robert, V.; Gornitzka, H; Martinez, A.; Dutasta, J.-P. *Angew. Chem., Int. Ed.* **2012**, *51*, 504−508.
(69) (a) Dawson, R. E.; Hennig, A.; Weimann, D. P.; Emery, D.; Ravikumar, V.; Montenegro, J.; Takeuchi, T.; Gabutti, S.; Mayor, M.; Mareda, J.; Schalley, C. A.; Matile, S. *Nat. Chem.* **2010**, *2*, 533−538. (b) Gorteau, V.; Bollot, G.; Mareda, J.; Perez-Velasco, A.; Matile, S.; Mareda, J. *J. Am. Chem. Soc.* **2006**, *128*, 14788−14789. (c) Gorteau, V.; Bollot, G.; Mareda, J.; Matile, S. *Org. Biomol. Chem.* **2007**, *5*, 3000−3012. (d) Matile, S. *Chem.—Eur. J.* **2009**, *15*, 28−37.
(70) (a) Estarellas, C.; Frontera, A.; Quiñonero, D.; Deyà, P. M. *Angew. Chem., Int. Ed.* **2011**, *50*, 415−418. (b) Estarellas, C.; Frontera, A.; Quiñonero, D.; Deyà, P. M. *Chem. Asian J.* **2011**, *6*, 2316−2318.
(71) Campos-Fernández, C. S.; Clérac, R.; Dunbar, K. R. *Angew. Chem., Int. Ed.* **1999**, *38*, 3477−3479.
(72) Campos-Fernández, C. S.; Clérac, R.; Koomen, J. M.; Russell, D. H.; Dunbar, K. R. *J. Am. Chem. Soc.* **2001**, *123*, 773−774.
(73) Campos-Fernández, C. S.; Schottel, B. L.; Chifotides, H. T.; Bera, J. K.; Bacsa, J.; Koomen, J. M.; Russell, D. H.; Dunbar, K. R. *J. Am. Chem. Soc.* **2005**, *127*, 12909−12923.
(74) Giles, I. D.; Chifotides, H. T.; Shatruk, M.; Dunbar, K. R. *Chem. Commun.* **2011**, *47*, 12604−12606.
(75) Geldard, J. F.; Lions, F. *J. Org. Chem.* **1965**, *30*, 318−319.
(76) Heintz, R. A.; Smith, J. A.; Szalay, P. S.; Weisgerber, A.; Dunbar, K. R. *Inorg. Synth.* **2002**, *33*, 75−121.
(77) van der Sluis, P.; Spek, A. L. *Acta Crystallogr. A* **1990**, *46*, 194−201.
(78) (a) Spek, A. L. *PLATON*; University of Utrecht: Utrecht, The Netherlands, 2008. (b) Spek, A. L. *Acta Crystallogr. D* **2009**, *65*, 148−155.
(79) Frisch, M. J.; et al. *Gaussian 09*, revision B.01; Gaussian Inc.: Wallingford, CT, 2010.
(80) Becke, A. D. *J. Chem. Phys.* **1993**, *98*, 5648−5652.
(81) Lee, C.; Yang, W.; Parr, R. G. *Phys. Rev. B* **1988**, *37*, 785−789.
(82) (a) McLean, A. D.; Chandler, G. S. *J. Chem. Phys.* **1980**, *72*, 5639−5648. (b) Krishnan, R.; Binkley, J. S.; Seeger, R.; Pople, J. A. *J. Chem. Phys.* **1980**, *72*, 650−654.
(83) Boys, S. F.; Bernardi, F. *Mol. Phys.* **1970**, *19*, 553−566.
(84) Escudero, D.; Frontera, A.; Quiñonero, D.; Deyà, P. M. *Chem. Phys. Lett.* **2008**, *455*, 325−330.
(85) Dennington, R. D., II; Keith, T. A.; Millam, J. M. *Agui 9.2.1*; Semichem, Inc.: Shawnee Mission, KS, 2008.
(86) Katz, B. A.; Strouse, C. E. *J. Am. Chem. Soc.* **1979**, *101*, 6214−6221.
(87) Funeriu, D. P.; Lehn, J.-M.; Fromm, K. M.; Fenske, D. *Chem.—Eur. J.* **2000**, *6*, 2103−2111.
(88) Manzano, B. R.; Zalón, F. A.; Ortiz, I. M.; Soriano, M. L.; Gómez de la Torre, F.; Elguero, J.; Maestro, M. A.; Mureiter, K.; Claridge, T. D. W. *Inorg. Chem.* **2008**, *47*, 413−428.
(89) Schnebeck, R.-D.; Freisinger, E.; Lippert, B. *Angew. Chem., Int. Ed.* **1999**, *38*, 168−171.
(90) Wang, G.-L.; Lin, Y.-J.; Jin, G.-X. *Chem.—Eur. J.* **2011**, *17*, 5578−5587.
(91) The metallacycles contain LS Fe(II) centers and are thus diamagnetic, which is supported by the Fe−N distances (ref 10c), the deep blue color of the complexes, and the magnetic susceptibility measurements. The metallacycles, however, albeit diamagnetic, exhibit a small percentage of paramagnetic contribution from HS iron atoms (∼5% of one Fe atom in each polygon); this results in broadening of the resonances in the NMR spectra. In particular, in the ^{19}F NMR spectrum of $[Fe_4(bptz)_4(CH_3CN)_8][BF_4]_8$, the coupling of ^{11}B and ^{10}B to the ^{19}F nuclei, with a relative ratio ∼4:1, is not observed (refs 10c and 98). Also, this contributes to the encapsulated $[PF_6]^-$ anions in $[Fe_5(bptz)_5(CH_3CN)_{10}][PF_6]_{10}$ exhibiting large upfield-shifted ^{19}F NMR resonances as compared to the free anions.
(92) Amouri, H.; Rager, M. N.; Cagnol, F.; Vaissermann, J. *Angew. Chem., Int. Ed.* **2001**, *40*, 3636−3638.
(93) Fleming, J. S.; Mann, K. L. V.; Carraz, C.-A.; Psillakis, E.; Jeffrey, J. C.; McCleverty, J. A.; Ward, M. D. *Angew. Chem., Int. Ed.* **1998**, *37*, 1279−1281.
(94) Paul, R. L.; Couchman, S. M.; Jeffery, J. C.; McCleverty, J. A.; Reeves, Z. R.; Ward, M. D. *J. Chem. Soc., Dalton Trans.* **2000**, 845−851.
(95) Glasson, C. R. K.; Meehan, G. V.; Clegg, J. K.; Lindoy, L. F.; Turner, P.; Duriska, M. B.; Willis, R. *Chem. Commun.* **2008**, 1190−1192.
(96) Paul, R. L.; Bell, Z. R.; Jeffery, J. C.; Harding, L. P.; McCleverty, J. A.; Ward, M. D. *Polyhedron* **2003**, *22*, 781−787.
(97) Bakhmutov, V. I. *Practical NMR Relaxation for Chemists*; John Wiley: Chichester, U.K., 2004.
(98) Paul, R. L.; Argent, S. P.; Jeffery, J. C.; Harding, L. P.; Lynam, J. M.; Ward, M. D. *Dalton Trans.* **2004**, 3453−3458.
(99) Nuclear Magnetic Resonance Spectroscopy in *Environmental Chemistry*; Nanny, M. A., Minera, R. A., Lecnheer, J. A., Eds.; Oxford University Press: Oxford, U.K., 1997; pp 65−66.
(100) Bakhmutov, V. I. Solid-State NMR in *Materials Science: Principles and Applications*; CRC Press: Boca Raton, FL, 2011−2012.
(101) Kaim, W. *Coord. Chem. Rev.* **2002**, *230*, 127−139.
(102) Kaim, W.; Kohlmann, S. *Inorg. Chem.* **1987**, *26*, 68−77.
(103) Guha, S.; Goodson, F. S.; Clark, R. J.; Saha, S. *CrystEngComm* **2012**, *14*, 1213−1215.
(104) Quiñonero, D.; Garau, C.; Frontera, A.; Ballester, P.; Costa, A.; Deyà, P. M. *J. Phys. Chem. A* **2005**, *109*, 4632−4637.
(105) Hay, B. P.; Bryantsev, V. S. *Chem. Commun.* **2008**, 2417−2428.
(106) Escudero, D.; Frontera, A.; Quiñonero, D.; Costa, A.; Ballester, P.; Deyà, P. M. *J. Chem. Theory Comput.* **2007**, *3*, 2098−2107.
(107) (a) Garau, C.; Quiñonero, D.; Frontera, A.; Escudero, D.; Ballester, P.; Costa, A.; Deyà, P. M. *Chem. Phys. Lett.* **2007**, *438*, 104−108. (b) Garau, C.; Quiñonero, D.; Frontera, A.; Costa, A.; Ballester, P.; Deyà, P. M. *Chem. Phys. Lett.* **2003**, *370*, 7−13.
(108) Garau, C.; Quiñonero, D.; Frontera, A.; Ballester, P.; Costa, A.; Deyà, P. M. *J. Phys. Chem. A* **2005**, *109*, 9341−9345.
(109) (a) Mingos, D. M. P.; Rohl, A. L. *Inorg. Chem.* **1991**, *30*, 3769−3771. (b) Mingos, D. M. P.; Rohl, A. L. *J. Chem. Soc., Dalton Trans.* **1991**, 3419−3425.
(110) Volume calculations for $[Fe_4(bptz)_4(CH_3CN)_8]^{8+}$ (56 Å^3) and $[Fe_5(bptz)_5(CH_3CN)_{10}]^{10+}$ (171 Å^3) were performed with the program *Voidoo* and a 1.4-Å-diameter rolling probe, which resulted in cavity occupancies of ∼68% and ∼83%, respectively.
(111) Hristova, Y. R.; Smulders, M. M.; Clegg, J. K.; Breiner, B.; Nitschke, J. R. *Chem. Sci.* **2011**, *2*, 638−641.
(112) Biros, S. M.; Yeh, R. M.; Raymond, K. N. *Angew. Chem., Int. Ed.* **2008**, *47*, 6062−6064.
(113) Kleywegt, G. J.; Jones, T. A. *Acta Crystallogr. D* **1994**, *50*, 178−185.
(114) Mercozzi, S.; Rebek, J., Jr. *Chem.—Eur. J.* **1998**, *4*, 1016−1022.
(115) Chierotti, M. R.; Gobetto, R. Solid-State NMR Studies on Supramolecular Chemistry in *Supramolecular Chemistry: From Molecules to Nanomaterials*; Steed, J. W., Gale, P. A., Eds.; John Wiley and Sons: New York, 2012; Vol. 2, pp 331−347.
(116) Ward, M. D. *Chem. Commun.* **2009**, 4487−4499.